Development and Inflight Validation of an Automated Flight Planning System Using Multiple-Sensor Windfield Estimation

by

Andrew Kevin Barrows

S.B., Aeronautics and Astronautics
Massachusetts Institute of Technology, 1989

Submitted to the Department of Aeronautics and Astronautics
in Partial Fulfillment of the Requirements for the Degree of

MASTER OF SCIENCE
in Aeronautics and Astronautics

at the
MASSACHUSETTS INSTITUTE OF TECHNOLOGY
June 1993

Signature of Author _____
Department of Aeronautics and Astronautics
May 7, 1993

Certified by _____
Associate Professor R. John Hansman
Department of Aeronautics and Astronautics
Thesis Supervisor

Accepted by _____
Professor Harold Y. Wachman
Chairman, Department Graduate Committee

Development and Inflight Validation of an Automated Flight Planning System Using Multiple-Sensor Windfield Estimation

by

Andrew Kevin Barrows

Submitted to the Department of Aeronautics and Astronautics
on May 7, 1993 in partial fulfillment of the requirements for the Degree of
Master of Science in Aeronautics and Astronautics

Abstract

Automated flight planning algorithms have been developed for aircrew decision aiding and primary mission control of autonomous air vehicles. Capabilities include multiple levels of strategic and tactical planning. These algorithms are typically evaluated in simulations where sensor performance and component integration are assumed to be ideal. In a practical system however, sensor fusion and component integration are likely to be performance- and cost-limiting factors. This project addressed fundamental integration issues through implementation of a multiple-level planning system on a microcomputer interfaced to various sensors, and flight testing onboard a single-engine general aviation aircraft.

Strategic flight plans were generated using a directed nodal search technique. Planning consisted of the minimum-time altitude profile over a great-circle route between two points, with the winds as the primary external influencing factor. Improvements made over existing trajectory planning algorithms included 1) introduction of virtual nodes at top-of-climb and top-of-descent points to allow highly accurate predictions of time enroute, and 2) addition of a time penalty on climb and descent legs to reflect the real costs associated with transitions in flight condition. Planning was based on a world model that included representations of winds and temperatures aloft, aircraft performance, ground facilities, and terrain. The wind and temperature model allowed real-time fusion of multiple-sensor data with forecast information to arrive at an improved estimate of atmospheric conditions. Flights made with intentionally-flawed initial wind forecasts showed that the system could quickly learn (through in-situ measurements) and adapt flight plans to actual conditions. Tactical planning algorithms that responded to a real or simulated collision hazard or engine failure were also successfully flight tested. After the tactical deviations, the system evaluated options to reacquire the original strategic plan or generate a new one. Flight testing indicated that, by increasing the computational power available, the planning system architecture is fundamentally adaptable to more complex flight planning problems. Probabilistic planning methods were introduced as a means of dealing with uncertainties in measurements and in the world model.

Thesis Supervisor: Dr. R. John Hansman

Title: Associate Professor of Aeronautics and Astronautics

Acknowledgments

My deepest gratitude goes to my mother Nancy and sister Kristen for their love and support. The high value placed on education by my family - including my father - is what really made this thesis happen.

Prof. John Hansman was my teacher, mentor, sounding board, and flight test pilot throughout this research. His insights, constructive criticism, and sound advice always challenged me to provide focus and direction to this project. Thanks for making me a better thinker, researcher, and writer!

I am indebted to Victor, Keiko, Paula, Jim, Adam, Ed, Alan, JP, Myk, Craig, Lee, Mark, Marc, and Amy, the graduate students of the M.I.T. Aeronautical Systems Laboratory, for a seemingly-endless stream of distractions and stimulating conversations. The late-night lab sessions will be remembered as some of the best times from graduate school! The efforts of the following students who assisted the project through M.I.T.'s Undergraduate Research Opportunities Program are also sincerely appreciated: Marc Amar, Andrew Belinky, Richard Brawn, Amy Gardner, Edward Hahn, Erik Larson, Trudy Liu, Andrew McFarland, Jeffrey Olson, and Oliver Sostre. Paul Bauer provided invaluable assistance as a flight test pilot and expert advisor on design of the flight test electronics.

Special thanks to John Araki, Sally Araki, T.J. Cradick, Ben DeSousa, Jack Kotovsky, Don Woodlock, the Necky Kayak Company, Korg Musical Instruments, Yamaha Musical Instruments, Aero Eagles Soccer, Nice Bumps Volleyball, 'Da Nasty and Bedside Prophets, Cessna Aircraft, Gary Fisher Mountain Bikes, Bridgestone Mountain Bikes, Spectrum HoloByte Software (makers of TETRIS™), Prof. Ed Crawley and the staff and students of Unified Engineering 1991-92, and Gus. Without them, this thesis would have been finished much, much sooner.

This research was supported by the Charles Stark Draper Laboratory under its Independent Research and Development Program.

Contents

List of Figures

List of Tables

Nomenclature

The meanings of variables and symbols used in this work are summarized here, with the chapters where they are used shown in parentheses.

A	segment time tailwind coupling matrix (Appendix C)
b	segment time constant vector (Appendix C)
C	wind measurement matrix (Appendix C)
$d_{T/C}$	distance to top of climb point (Appendix C)
d	vector of segment distances (Appendix C)
E	segment tailwind extraction matrix (Appendix C)
ETA	vector of waypoint estimated arrival times (Appendix C)
$f(n)$	cheapest cost from start node through node n to goal node (2)
$g(n)$	cost from start node to node n (2)
GS	groundspeed vector (3, Appendix C)
$h(n)$	heuristic function at node n (2)
K	Kalman gain matrix (Appendix C)
L	lower triangular matrix (Appendix C)
m_i	measurement/forecast flag for i-th meteorological datapoint (3)
n'	successor of node n (2)
R_{ij}	(i, j) element of wind correlation matrix (Appendix C)
r	reference point for wind and temperature retrieval (3)
$\mathbf{r}_i$	location of i-th meteorological datapoint (3)
ROC	vector of segment climb rates (Appendix C)
s	start node (2)
ST	vector of segment thicknesses (Appendix C)
t	reference time for wind and temperature retrieval (3)
t_i	time when i-th meteorological datapoint was generated (3)
t	vector of segment times (Appendix C)
TAS	true airspeed vector (3, Appendix C)
TW	vector of segment tailwinds (Appendix C)

u_i	i-th component of wind fluctuation vector (Appendix C)
v	scalar variable retrieved from meteorological model (3)
v_i	value of v at i-th meteorological datapoint (3)
w_i	weighting of i-th meteorological datapoint (3)
W_{hi}	horizontal weighting of i-th meteorological datapoint (3)
W_{mi}	measurement weighting of i-th meteorological datapoint (3)
W_{ti}	time weighting of i-th meteorological datapoint (3)
W_{vi}	vertical weighting of i-th meteorological datapoint (3)
$\mathbf{W}$	wind vector (3)
$\mathbf{x}$	wind forecast vector (Appendix C)
$\mathbf{x}^-$	a priori mean wind forecast vector (Appendix C)
$\mathbf{x}^+$	a posteriori mean wind forecast vector (Appendix C)
$\mathbf{z}$	vector of wind measurements (Appendix C)
θ_{ij}	(i, j) element of wind power spectral density matrix (Appendix C)
θ	white noise vector (Appendix C)
Θ	white noise covariance matrix (Appendix C)
σ_h	horizontal weighting shape factor (3)
σ_v	altitude weighting shape factor (3)
$\Sigma(\mathbf{TW})$	covariance matrix of segment tailwinds (Appendix C)
Σ	wind forecast covariance matrix (Appendix C)
Σ^-	a priori wind forecast covariance matrix (Appendix C)
Σ^+	a posteriori wind forecast covariance matrix (Appendix C)
τ	time displacement (Appendix C)
ξ	spatial displacement vector (Appendix C)
ω	time frequency (Appendix C)
Ω	spatial frequency vector (Appendix C)

1 Introduction

1.1 Automated Flight Planning Systems

Flight planning algorithms have been developed for generating dynamic mission plans that govern flight routing and resource allocation. These algorithms can be used as decision aids by flight crews or function as the mission controller on an autonomous air vehicle. Planning may be done at the strategic level (e.g. generating minimum-fuel or minimum-time flight trajectories) or tactically, in response to unpredicted situations (e.g. a loss of power or another aircraft posing a collision hazard).

These systems base plans on dynamic world models of the factors that affect a flight. Wind, storm activity, turbulence, icing, positions of nearby aircraft, and many other factors evolve in ways that are not fully known or determined before the flight begins. Models rely on a combination of forecast information and direct measurements

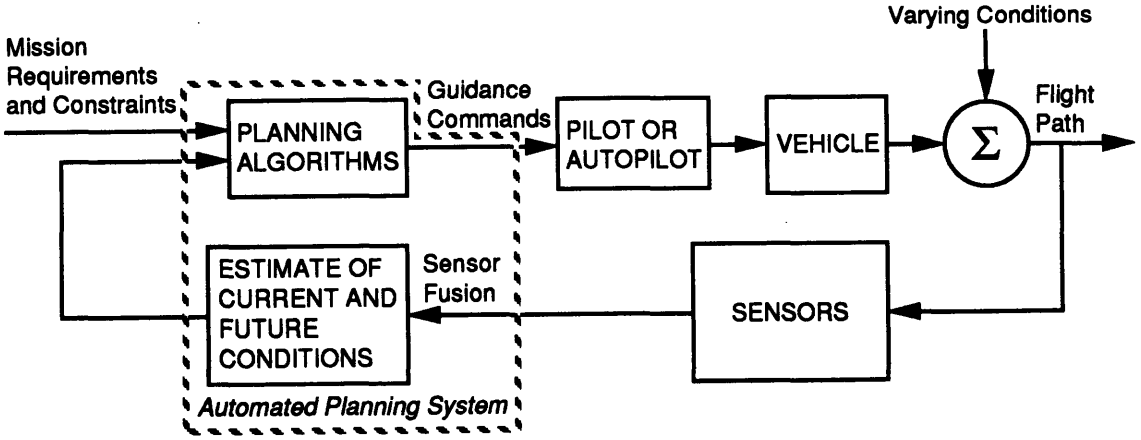

Figure 1.1 Automated Planning System Integration

of these variables to accurately reflect actual conditions. *Sensor fusion* consists of integrating measurements into prior estimates to intelligently update these models. Planning algorithms are then used to generate guidance commands based on these models. If mission planning can be thought of as the outermost guidance loop in aircraft flight, then planning algorithms with fused sensor information "close the outer guidance loop," as illustrated in Figure 1.1.

1.2 Previous Research

Much work has been done on developing algorithms designed to aid in flight planning and resource allocation. Simple route optimizations were being performed on ground-based computers in the mid 1960s [Rose, Simpson et al.]. More recently, studies of integrated decision-aiding systems [Corrigan and Keller, Glickstein], and pilot-vehicle interface issues [Layton et al.] have been conducted.

The role of automated flight planning algorithms for autonomous air vehicles (AAVs) has received much attention [Adams and Hansman]. Planning algorithms will perform flight routing and high-level mission control for AAVs, either alone or in coordinated squadrons. Current unmanned air vehicle systems typically require a human operator during some portion of flight (e.g. landing) and follow an "open-loop" preprogrammed set of commands for routing and resource allocation.

Military applications studied have included reconnaissance, target selection and ordering, route planning, and munitions use. Additional factors taken into account typically include exposure to threats such as surface-to-air missile sites, effectiveness in destroying a target, terrain radar masking, radar cross section exposure, and a host of others.

1.3 Problem Statement and Objective

Research on automated planning systems has relied heavily on laboratory simulations where sensor performance and component integration are assumed to be ideal. In a practical planning system however, issues such as sensor fusion and component integration are likely to be performance-limiting or cost-limiting factors. However, the difficulty and high cost of flight testing has limited the amount of work done in this area. This experimental effort addressed the need for flight testing of operational planning systems. The goal of this project was to identify fundamental system integration issues through implementation of a flight planning system using real-time sensor measurements on an actual vehicle.

Automated planning software, flight-ready computer and sensor hardware, and a flight test program were developed for this investigation. Flight testing was done on a single-engine light aircraft under visual flight rules (VFR) in the New England region. Tests dealt with planning of a straight-line trajectory between two points, yielding a two-dimensional problem (distance along a line and altitude) with the wind being the primary environmental factor that influenced the problem. The ability of the system to react to unexpected situations was also investigated by implementing algorithms that could generate tactical responses to traffic hazard and power loss situations. These simplified problems retained the important features of more general problems (unpredictable events and imperfect knowledge of aircraft performance and environmental conditions), permitting identification of sensor fusion and system integration issues without unnecessary complications. The structure of the automated planning system is shown in Figure 1.2.

The planning algorithms accepted sensor data, propulsion status, and traffic status as inputs along with user commands to generate textual guidance commands for the pilot. Wind measurements (made by comparing airspeed and groundspeed vectors) were

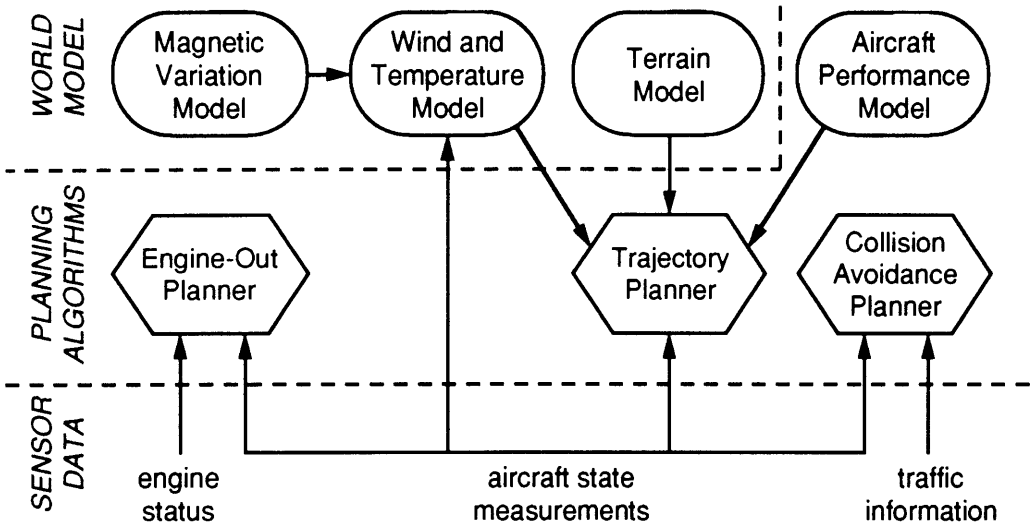

Figure 1.2 Planning System Structure

taken periodically and then fused into the wind and temperature model. Models of terrain and magnetic variation were also used by the planning algorithms. These models taken together form the *world model* on which the planning algorithms operated. A performance model of the test aircraft was also employed by the planning system.

1.4 Planning Algorithms

Planning systems typically employ a hierarchical structure separating the planning problem into global and more detailed components that represent multiple levels in the planning process. These sub-tasks tend to fall within a spectrum of planning processes that range from strategic to tactical in nature.

1.4.1 Strategic Planning

Strategic planning affects long-range optimality of the flight in a global manner. For a mission with multiple stops or targets, selection and ordering of objectives constitutes part of the strategic planning process. Strategic planning also includes generation of flight trajectories defined as sets of waypoints and/or schedules of airspeeds, climb rates, control inputs, etc.

For this project, a strategic trajectory planner was implemented that found the minimum-time path between two points. The winds aloft and aircraft performance were the primary factors affecting the optimum strategic plan. The planning algorithm was based on techniques derived from directed search methods. These methods typically operate on a network of "nodes" that represent different stages in solving a problem. Such techniques search the paths leading from the starting node to the "goal" node, with the ultimate objective of finding the path which minimizes a specified cost function. The nodal network for the flight planning problem, depicted in Figure 1.3, filled the airspace between the starting point and the destination airport. The cost function optimized was a linear combination of the total fuel burn and trip duration. In addition to this cost function, a "hard" constraint was imposed on fuel burn since it is limited by the maximum fuel load of the airplane.

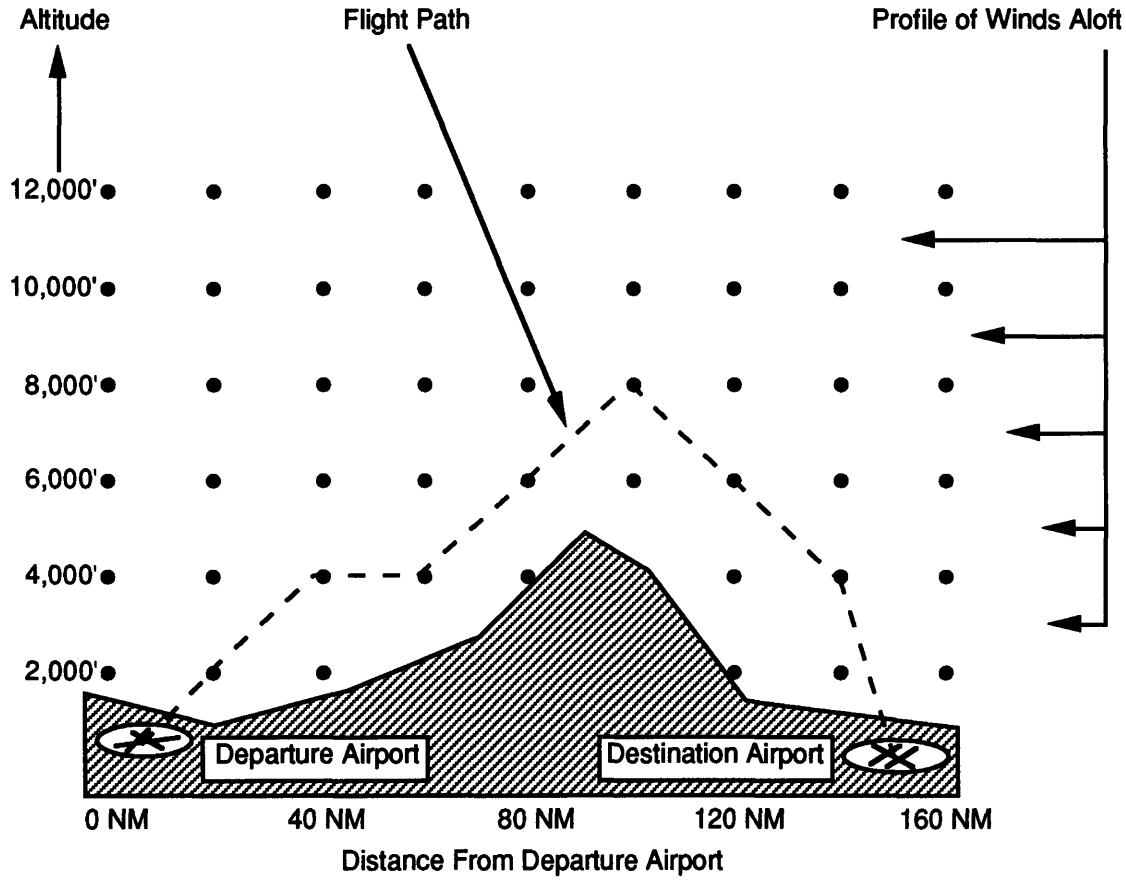

Figure 1.3 Flight Planning Problem

1.4.2 Tactical Planning

Tactical planning includes short-term procedures necessary to deal with unexpected, unpredicted, or emergency situations. Situations which require tactical planning tend to last for only a fraction of the flight duration, but may have implications for the remainder of the flight. Examples include deviations around thunderstorms and altitude transitions to escape turbulence and icing. Autonomous aircraft will need the capability to generate plans to escape populated areas in the event of an equipment failure. This has been identified as critical to the acceptance of AAVs for civilian applications [Adams and Hansman].

This project investigated performance of a tactical planner to generate maneuvers to avoid nearby traffic. When a real or simulated traffic encounter ended, the pilot could recapture the original strategic flight plan or - if the tactical maneuver left the aircraft significantly off the original plan - a new strategic plan could be generated. A second tactical planner was implemented to provide guidance to a suitable airport after a simulated engine failure in the single-engine test aircraft.

1.5 Sensor Fusion

The modeled environmental variables which influence a flight range from constantly changing factors, such as the windfield, to factors which are essentially constant, such as terrain and ground facilities (i.e. airport locations and runway information). Accuracy of these static and dynamic world models is key to the success of a planning system; optimized trajectories are only as good as the assumptions on which they are based.

The winds aloft have a fundamental effect on the desirability of one flight altitude over another. The optimum routing and altitude profile is a complex balance between aircraft performance, the windfield, terrain features, and the length of the flight. Since

the windfield constantly changes on time scales comparable to or shorter than a typical flight, it is necessary to use a *dynamic* representation capable of representing variations of these quantities.

While forecasts of these changing variables are readily available, the well-documented decrease in accuracy over time of winds aloft forecasts [Hollister et al.] dictates that current wind measurements are a necessary supplement to forecast values for flight planning. Forecast information still has great value, however, especially for points and times near which no measurements are available. Both types of information clearly have their place in a complete atmospheric description, so that a scheme such as the one outlined in Figure 1.4 is needed for intelligently fusing sensor measurements into an existing forecast to arrive at an updated estimate of present and future conditions.

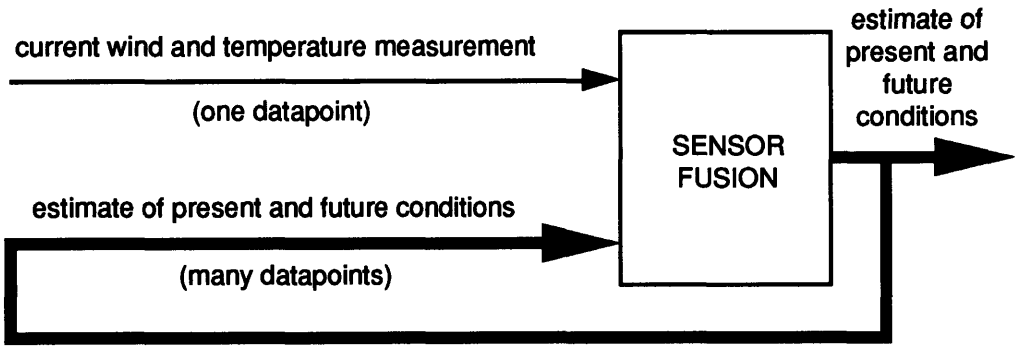

Figure 1.4 Fusion of Sensor Data

An aircraft using advanced flight planning algorithms can make periodic wind and temperature measurements to improve its meteorological model, or even use data obtained from external sources such as balloon soundings and wind profilers. The technology now exists to send aircraft-based measurements via datalink [Benjamin et al.] to a ground facility or other aircraft where multiple measurements can be fused with a forecast to form a current estimate of meteorological conditions. The success of a planning system's dynamic wind model, and hence of the planning system as a whole, is limited by methods used for sensor fusion.

The flight test system's dynamic wind and temperature model used a weighted averaging scheme to fuse inflight measurements into existing estimates of these variables. This method applied a weighting to each datapoint according to its distance (in time and space) from the point and time where wind and temperature were to be estimated. Nearby datapoints had a strong influence on wind and temperature estimates, while distant datapoints carried very little weight.

1.6 Mission Management

The highest level of decision making, the *mission management* level, coordinates the multiple levels of strategic and tactical planning. The mission management role includes monitoring of the current flight plan to determine if it is satisfactory or, if it is not, initiating the strategic replanning process. When an unexpected condition requires a short-term change to the flight plan, the mission manager initiates creation of a tactical deviation from the planned trajectory. After a tactical maneuver, it determines whether to reacquire the original strategic plan or to generate a new one. During flight tests, the test engineer and pilot performed the mission management function by using lower-level strategic and tactical planners as decision aids. AAV applications will require dedicated mission management algorithms.

1.7 Overview

Details on the planning algorithms and world model elements used in flight testing are given in Chapters 2 and 3. Chapter 4 describes the novel, inexpensive approach used for flight testing including the test aircraft, computer, and sensing hardware. Chapters 5 and 6 present and discuss data from flight testing of strategic and tactical planning algorithms. Conclusions of this work are presented in Chapter 7.

Appendix A is an algorithmic description of the uniform-cost search method used by the trajectory planner, and Appendix B contains performance curves used by the

aircraft performance model. A probabilistic wind model and application examples are presented in Appendix C.

2 Planning Algorithms

This chapter details the strategic trajectory planner and the aircraft performance model used to calculate flight plan costs. Probabilistic planning methods are then discussed. Finally, the tactical engine-out and collision avoidance planners are described.

2.1 Trajectory Planner

The strategic trajectory planner generated altitude profiles over the great-circle route between a starting point (this could be an airport or a point in the air) and the destination airport. Textual output to the pilot consisted of a set of waypoints, crossing altitudes, and ETAs. The pilot flew the commanded altitude profile by initiating climbs and descents at appropriate points specified by the planner. The next five sections provide details on the trajectory planner.

2.2 Search Method

2.2.1 Directed Search Methods

The strategic trajectory planner used a *directed search* method to find the minimum-cost path through the two-dimensional nodal network shown in Figure 1.3. By avoiding repetitive calculations, directed searches provide an efficient way for systematically evaluating paths from the starting node to the destination node. Two such methods are described below.

2.2.2 *Uniform-Cost Search*

The directed search method used by the planner was the *uniform-cost* search, which is categorized in the literature under the more general family of *best-first* searches [Pearl, Nilsson]. Best-first searches operate by keeping track of the cheapest path cost $g(n)$ found thus far from the start node to each node n. A loop through the iterative procedure consists of selecting the node with the lowest cost $g(n)$ and then *expanding* it, by exploring *arcs* leading away from n to other nodes. When exploring these node-to-node arcs, the search considers nearby *successor* nodes on the level, climb, and descent paths leading away from n. The cost of traversing the arcs between node n and each successor n' is calculated and then added to $g(n)$ to find $g(n')$ for each successor. The node with the lowest cost is then expanded to begin another loop. The process repeats as the search moves forward from the start node through the nodal network until the destination node is reached. Pointers are used to keep track of the solution path, with successor nodes pointing back to their *parent* nodes. A step-by-step algorithmic description of the uniform-cost search is given in Appendix A.

As the size of the search network increases, the time required to perform a uniform-cost search increases rapidly. The uniform-cost search was adequate for simple flight planning problems, but solving problems more complicated than the one addressed by this project will require a faster search algorithm.

2.2.3 *A* Search*

The uniform-cost search may be significantly sped up by the introduction of a carefully-selected *heuristic function*. This function $h(n)$ is an "educated estimate" of the cost from node n to the goal node and is added to $g(n)$:

$$f(n) = g(n) + h(n) \tag{2.1}$$

to arrive at $f(n)$, an estimate of the cost of the cheapest path from the start to the goal *that is constrained to go through node n.* Using this new estimate $f(n)$ as the node expansion criterion in the uniform-cost search results in the A^* (pronounced A-star) search. If $h(n)$ is chosen to always give an optimistic (i.e. low) estimate of the cost from n to the goal, the search is guaranteed to find the minimum-cost solution path. Use of a well-chosen heuristic results in a directed search that avoids spending computational time exploring arcs that are not part of the optimum solution.

The A* search has been applied successfully to trajectory planning problems [Niiya, Corrigan and Keller] and was used as the framework for the flight planning algorithm. Since the planner was sufficiently fast for flight test purposes (maximum planning time of 40 seconds), the heuristic function was set to zero, resulting in a uniform-cost search.

2.3 Node Network

The trajectory planning problem was defined in two spatial dimensions: distance along a line and altitude. Nodes were distributed on a two-dimensional grid with 11 horizontal positions and 11 vertical levels. The horizontal positions were at the start position and destination airport, with the remaining nine points evenly distributed between the two endpoints. Node altitudes included the VFR cruising altitudes appropriate to the direction of flight, and 500-foot levels at and below 3000 feet. Altitudes above 12500' were not included since they were above the practical altitude range of the test aircraft (see Table 2.1).

After the grid was constructed, nodes at the start and destination altitudes were patched into the grid at their respective positions. Finally, *exclusion zones* were imposed to account for terrain. Any node fewer than 1000 feet above ground level was removed from the network to ensure that flights would not be planned hazardously close to the

Table 2.1 Node Altitudes

Eastbound Ground Track (0°-179° magnetic)	Westbound Ground Track (180°-359° magnetic)
500'	500'
1000'	1000'
1500'	1500'
2000'	2000'
2500'	2500'
3000'	3000'
3500'	4500'
5500'	6500'
7500'	8500'
9500'	10500'
11500'	12500'

ground. To allow departures and approaches at airports, nodes at and directly above the start and destination nodes were not removed.

2.4 Aircraft Performance Model

Arc costs were based on a performance model of the test aircraft. This model was represented as curve fits describing the following performance curves in the *Arrow IV Pilot's Operating Handbook* [Piper Aircraft]:

> FUEL, TIME, AND DISTANCE TO CLIMB
> *Associated Conditions: Power - 2700 RPM, Full Throttle, Climb Speed - 90 KIAS*
>
> SPEED POWER PERFORMANCE CRUISE
> *Associated Conditions: Power - 2400 RPM, 65% or Full Throttle above 9500' Density Altitude*
>
> FUEL, TIME, AND DISTANCE TO DESCEND
> *Associated Conditions: Power - 2400 RPM, Throttle as Required, Descent Speed - 146 KIAS*

These curves are reproduced in Appendix B. The curves represented the standard climb, cruise, and descent flight conditions used throughout the flight test program. Although density altitude and aircraft weight were specified as inputs to the performance model, the curves were assumed to be insensitive to weight. This was a good assumption for light piston aircraft with their typically small (less than 0.2) fuel weight fractions.

Functional forms for the performance equations were verified in flight tests exploring several regimes of interest within the aircraft performance envelope.

Since performance characteristics remained effectively constant over the course of a single flight, a static performance model was used. In practice, aircraft performance changes over a period of years, usually due to deterioration in engine performance and condition of the aerodynamic surfaces. A quasi-static performance model can be gradually changed over the lifetime of the aircraft to reflect its varying performance. This can be done by performing periodic performance flight testing, or by a more sophisticated scheme which continually updates a dynamic performance model during routine aircraft operation.

2.5 Cost Function

The cost function was implemented to allow any linear additive combination of trip duration and fuel burn. In practice, fuel burn was not weighted due to the difficulty of obtaining accurate measurements of this variable for the test aircraft. Therefore, during flight tests the planner was configured to provide flight plans optimized for minimum time.

2.6 Distinguishing Features of The Flight Planning Problem

This section discusses several adaptations made to standard directed search techniques in order to reflect unique characteristics of the flight planning problem.

2.6.1 Variance of Connectivity With State

In most directed search applications, a node's successors can be determined before the search begins; one can tell which nodes are *reachable* from a given node before any costs are calculated. This was not the case with the flight planning problem considered here, since node connectivity varied with the states of the aircraft and

atmosphere. As an example, consider a climb arc between two nodes (Figure 2.1). Under certain wind conditions it might have been possible to accomplish this climb - node B was "reachable" from node A.

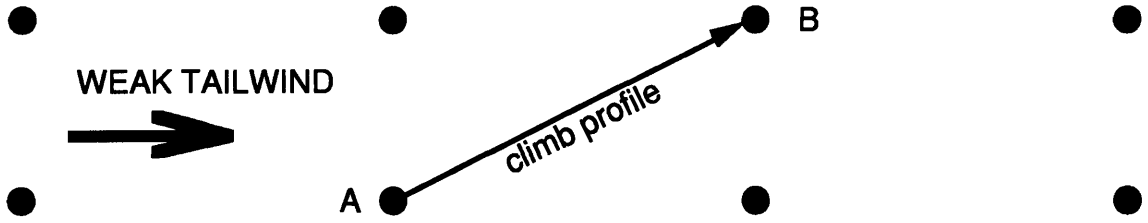

Figure 2.1 Node Connectivity - Node B Reachable From Node A

However, if there were a strong tailwind as in Figure 2.2, it may not have been possible to reach the final altitude before passing the position of node B (the aircraft would have been blown under node B). In order to retrieve the correct value of the

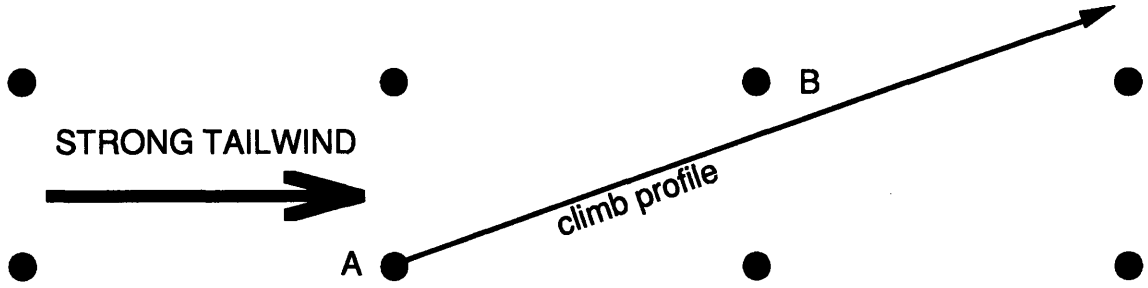

Figure 2.2 Node Connectivity - Node B Unreachable From Node A

time-varying wind from the wind model, it was necessary to know when the aircraft would be flying along a given arc. Therefore, the estimated time was stored at each node by the search algorithm to allow real-time determination of node connectivity.

2.6.2 Variance of Cost Function With State

Arc costs, in addition to node connectivity, were dependent on the state of the aircraft and atmosphere. The primary state variable affecting the time cost of a given arc was the headwind or tailwind component. The estimated time stored at each node was used to make real-time arc cost calculations based on winds when the arc was traversed.

2.6.3 Breakdown of Climb and Descent Arcs

Arcs involving climbs or descents were broken into two components: a climb or descent segment, and a level segment. An example climb arc is shown in Figure 2.3. Without this breakdown scheme, the planner would have had to assume a climb profile (shown as a dashed line) at non-standard power, airspeed, and climb rate conditions. (These control inputs would have been chosen to ensure that the climb profile intersected node B.) However, since typical aircraft operations are based on standard flight

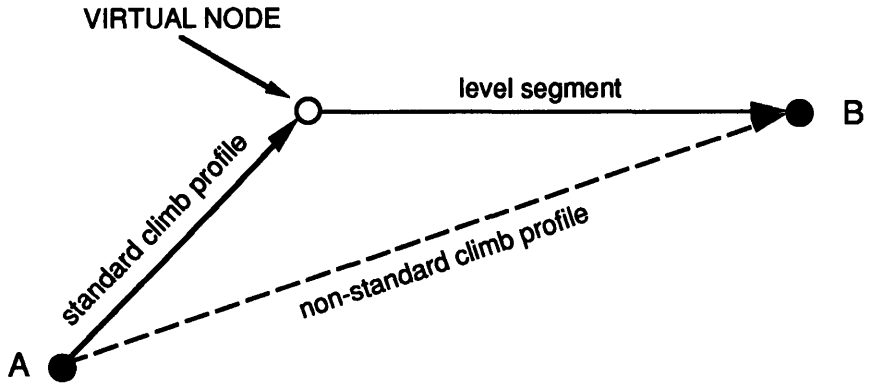

Figure 2.3 Breakdown of Climb Leg From Node A to Node B

conditions, it was desirable for the planner to adhere to these practical constraints. To allow a standard climb profile (corresponding to the airspeed and power settings in the aircraft performance model), a *virtual node* was created at the point where the standard profile intersected the altitude of node B. Standard cruise airspeed and power settings were assumed on the level segment. Different wind values were retrieved from the wind model for the two segments, allowing very accurate calculation of arc costs.

2.6.4 Altitude Transition Penalty

It was observed during preliminary flight testing that certain wind profiles could lead to plans that contained alternating climbs and descents in rapid succession. For example, small variations in the windfield structure might have caused the optimum altitude to oscillate between two altitudes (e.g. 5500' and 7500'). This tended to occur

when the wind component along the direction of flight was relatively constant with altitude. In such circumstances the time differences associated with cruising at one altitude versus another were relatively small, so that minor horizontal windfield variations could cause the optimum flight altitude to oscillate.

There is no doubt that these plans were the minimum-time profiles consistent with the estimated windfield and the specified cost function. However, there are inefficiencies associated with transitions in flight condition which were not modeled by the performance curves used to describe the aircraft. For example, when the aircraft was transitioned between climb, cruise, and descent conditions, there were periods of acceleration and deceleration during which the aircraft was not at the optimum speed for the current condition. It was clear that these transitions represented a real cost which should be considered in planning. For manned missions, there are additional crew workload costs associated with transitions in flight condition. Therefore, an altitude transition penalty was added to the cost function for node-to-node arcs which included a climb or descent. The value of 12 seconds was determined empirically by planning flights using a simulated wind profile that was nearly constant with altitude. The transition penalty time was increased from zero until the optimum plans no longer contained multiple climb/descent cycles. This altitude transition penalty worked well in practice; during flight testing, the planner did not generate profiles with repetitive climbs and descents.

2.7 Probabilistic Planning

The transition penalty was instituted to account for factors not captured by the aircraft performance model. The atmosphere is an even more complex system, possessing many characteristics which cannot be modeled deterministically by existing tools. As with unmodeled performance features, uncertainties in the winds aloft have real effects on costs optimized by the planner. (These may be cost penalties or cost *savings*;

sometimes the conditions are more favorable than predicted.) The planning methods above make no attempt at dealing with this uncertainty. Instead, they plan deterministically by assuming that the wind model is an exact description of present and future conditions.

Accounting for measurement and modeling uncertainty is expected to yield lower operational costs when averaged over the course of many flights. This approach requires planning and sensor fusion methods fundamentally different from those previously mentioned. Instead of finding the single optimum path through a deterministic windfield, a probabilistic planner considers multiple plans and the probabilistic nature of their costs. For example, when choosing among several cruise altitudes, a probabilistic planner calculates the probability density function (PDF) of the cost associated with each altitude. An expected-value criterion is then applied to choose the cruise altitude which yields the lowest average cost. These PDFs change during a given flight as measurements are made, letting evidence build in favor of keeping or changing the current flight plan.

Probabilistic solution techniques typically break a problem into stages, just as the trajectory planner broke the flight into node-to-node arcs. At each stage of the problem, all possible environmental conditions (e.g. a PDF of windspeeds that might be encountered) are considered along with all possible actions (e.g. fly level, initiate a climb, or initiate a descent) to arrive at a choice that minimizes the expected value of a cost function. A prospective flight plan is adopted when its mean cost falls below that of the current plan. A framework for probabilistic representations of planning problems is offered by the field of *decision analysis* [Drake and Keeney].

Probabilistic planning also requires a probabilistic description of cost-influencing environmental factors and their interrelationships. For example, a probabilistic wind model describes not only the wind components themselves, but also covariances between the winds at different locations and times. A probabilistic wind modeling technique was

developed and is presented in Appendix C. Implementation of such a model requires significant processing capability to handle the large data sets which describe the variances and covariances of atmospheric variables. Planning algorithms which deal with this uncertainty are also significantly more complex, requiring representation of many possible environmental conditions and choices at each stage of a flight. Due to limitations of the microcomputer used, the flight test program did not include probabilistic planning.

2.8 Collision Avoidance Planner

The collision avoidance planner generated tactical deviations in response to real or simulated warnings from a Traffic Collision Avoidance Device (TCAD) or Traffic Alert and Collision Avoidance System (TCAS). When this mode was invoked, strategic planning was suspended and the user was issued a traffic avoidance maneuver. For simplicity, only climbing and descending maneuvers were commanded. When the collision threat had been resolved, the user could either reacquire the original flight plan or replan a new flight profile.

2.9 Engine-Out Planner

The tactical engine-out planner could be used during actual or simulated power loss events to provide guidance to a nearby airport. Given aircraft position and altitude, the engine-out planner searched a database for airports within gliding distance. An airport was considered usable if the aircraft was predicted to be at 500 feet or higher over the field, ensuring that a suitable landing pattern could be set up as the airport was approached. If there were multiple airports satisfying this criterion, the airport with the highest predicted altitude over the field was designated as the primary airport. Updated magnetic bearing and distance to the primary airport were given to the pilot every 10 seconds.

3 World Model

The various elements of the world model used by the planning system are described here. The world model included representations of wind, temperature, magnetic variation, and terrain.

3.1 Wind and Temperature Model

The dynamic meteorological model represented wind and temperature as functions of latitude, longitude, altitude, and time. The model was initialized with forecast information and updated in flight with fused sensor measurements. Representation of atmospheric field variables was made difficult by the fact that the available measurements and forecast datapoints were randomly distributed in space and time; datapoints tended not to fall onto a structured grid of times and locations. For instance, aircraft-based measurements were made at scattered locations and times along the flight path, and forecasts were specified at reporting stations that were not evenly spaced. A filtering scheme was therefore needed to estimate wind and temperature *between* stations - or between times at which data was specified. Such a method is referred to as an *objective analysis* in the meteorological literature.

The wind and temperature model employed a weighted averaging scheme based on the Barnes objective analysis for mesoscale datafields [Barnes]. The model was initialized before each flight with forecast datapoints numerically generated by the National Weather Service. The forecast profile at a reporting station was received as a

"stack" of wind and temperature datapoints at various altitudes (3000', 6000', 9000', and 12000' were used in flight testing). These forecast datapoints were only valid over a specified interval of several hours, so a time series of datapoints was specified at every reporting station and altitude. Forecast information was also tagged with the time when the numerical model was actually run, allowing computation of the "age" of a forecast datapoint. Inflight measurements were incorporated as single datapoints with a specific horizontal position, altitude, and time of measurement. Individual forecast and measured datapoints were handled in the same way by the model; a forecast datapoint was averaged into a wind estimate just like an inflight measurement. However, the weighting functions for these two classes of data were different, reflecting their distinct properties.

3.1.1 Weighted Averaging Scheme

Wind and temperature were estimated as weighted averages of the n forecast and measured datapoints in the model. The west-to-east wind component, south-to-north wind component, and temperature were handled as separate scalar variables. The formula used to estimate scalar variable v at location $\mathbf{r}$ and time t (called the *reference location* and *time*) was:

$$v(\mathbf{r}, t) = \frac{\sum_{i=1}^{n} v_i w_i(\mathbf{r}_i - \mathbf{r}, t_i - t, m_i)}{\sum_{i=1}^{n} w_i(\mathbf{r}_i - \mathbf{r}, t_i - t, m_i)} \tag{3.1}$$

where v_i is the value of v at the i-th datapoint and w_i is the weight given to the i-th datapoint. The weighting given to a datapoint was a multiplicative combination of the following weighting factors:

W_h: horizontal displacement of the datapoint location, $\mathbf{r}_i$, from the reference location

W_v: vertical displacement of the datapoint from the reference altitude

W_t: time difference between when the datapoint was generated, t_i, and the reference time

W_m: whether the datapoint was measured or forecast (indicated by m_i)

Nearby datapoints (in space and time) generally had a strong influence on local wind and temperature estimates, while distant datapoints carried very little weight. The components of $w = W_h W_v W_t W_m$ are described below.

3.1.2 Horizontal Weighting

The horizontal weighting function, like that used in the Barnes objective analysis [Barnes], was a Gaussian-shaped function of distance:

$$W_{hi} = \exp\left(-\frac{|\mathbf{r}_i - \mathbf{r}|^2}{2\sigma_h^2}\right) \tag{3.2}$$

This weighting function drops off with distance at a rate determined by σ_h. Excessively large values of σ_h resulted in overly smoothed estimates, while choosing σ_h too small produced detail near datapoints but yielded an excessive loss of structure between datapoints.

The value of σ_{hf} for forecasts was chosen as 40 nm to give a horizontal weighting of approximately 0.5 midway between reporting stations, which have an average spacing of 80-120 nm in the New England flight test region.

For measurements, σ_{hm} was set to 30 nm based on the expected 15 nm spacing between inflight wind measurement points. This lower value of σ_h gave measured datapoints smaller regions of influence than forecast datapoints.

3.1.3 Altitude Weighting

The altitude weighting, W_v, for measurements was a Gaussian function of altitude similar to the horizontal weighting in equation (3.2). The value of σ_{vm} = 2500 feet was

determined empirically by comparing the results of using different values on typical wind profiles.

Since forecast datapoints were disseminated in "stacks," a linear interpolation scheme - as opposed to a smoothing method based on Gaussian weighting - was used for forecast datapoints in the vertical dimension. For example, if the reference was at 4000 feet, a forecast datapoint at 3000 feet was given a weight of $W_v = 2/3$, a datapoint at 6000 feet was given a 1/3 weighting, and datapoints at 9000 and 12000 feet were assigned $W_v = 0$. For reference altitudes below 3000 feet, values were linearly extrapolated based on forecast datapoints at 3000 and 6000 feet.

3.1.4 Time Weighting

As a datapoint grew older, its temporal weighting was decreased to reduce its influence on wind and temperature estimates. The "age" of a datapoint (whether measured or forecast) was computed as the difference between the reference time and the time when the datapoint was generated, and then used as an argument to the time weighting function, W_t. This function, shown in Figure 3.1, is an exponential decay from 1.0 to 0.5 with a time constant of 2 hours.

3.1.5 Measurement Weighting

Measurements provide a better description of the wind and temperature at a given point and time than do values estimated from forecast information. In regions near measurement points, it was essential that the model reflect measured values - not forecast values. An additional weighting factor, W_m, was therefore applied to measured datapoints to influence wind and temperature estimates in favor of measurements. The weighting of $W_m = 3.0$ was determined empirically by comparing effects of various weightings on fusion of measurements into typical wind profiles. This value provided a

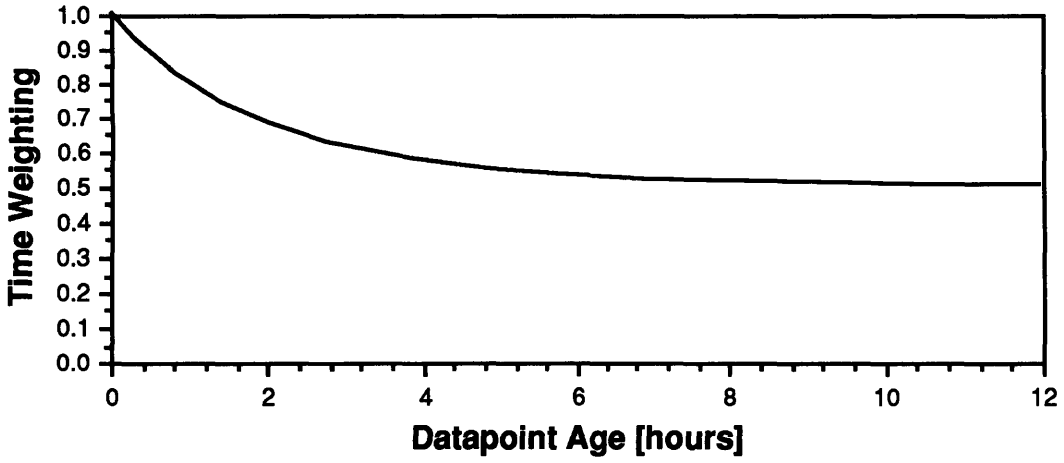

Figure 3.1 Time Weighting Function

balance between the model not reflecting off-forecast conditions (if the measurement weighting was too small) and the model ignoring valuable forecast information (if the measurement weighting was too high)

W_m was simply set to 1.0 for forecast datapoints in order to produce the correct relative weighting between forecast and measured values.

3.2 Magnetic Variation Model

The world model also included a representation of magnetic variation used for fusion of wind direction measurements into the wind and temperature model. Wind measurements made in the aircraft were relative to magnetic north, because this was the format in which the navigational instruments output ground track and heading. Since winds aloft forecasts were disseminated with directions relative to true north, magnetic variation values were needed to convert magnetic headings to true headings for representation by the wind model. A planar fit to magnetic variation values on the northern half of the December 1986 NOAA New York sectional chart was developed. This static magnetic variation model was accurate to within 0.15 degrees in the New England flight test region.

3.3 Terrain Model

To ensure safe terrain clearance, a static terrain model was used to generate exclusion zones for the planner nodal structure. This prevented planned flight profiles from passing closer than 1000 feet from the ground, except on departure and approach paths near airports. Terrain datapoints along the flight test routes were typically spaced five nautical miles apart, with extra datapoints added to account for radio towers, mountain ridges, and other local elevation maxima.

4 Flight Test Hardware

To perform the planning, world modeling, and measurement functions described previously, a self-contained system consisting of a microcomputer interfaced to various air data sensors was constructed for use in a light piston aircraft. The system was contained within a pallet that mounted in the rear seat of the airplane and functioned independently of the aircraft's systems. The result was a simple inexpensive testbed for flight testing of automated planning systems with integrated sensors. This scheme also permitted use of the computer as a simulation facility for development of planning software. This chapter describes the aircraft and flight hardware used for the test program.

4.1 Test Aircraft

The test aircraft shown in Figure 4.1 was a normally-aspirated single-engine, retractable-gear, four-place Piper Arrow IV. The Arrow was particularly attractive for flight testing due to its relatively low operating cost and minimal test crew requirements (flight tests required a pilot, a test engineer, and no ground personnel).

4.2 Flight Hardware

The instrumentation, shown schematically in Figure 4.2 and described in the following subsections, included a computer to run flight planning and data acquisition software, sensing instruments, power supplies, and a battery. The sensing package had a LORAN receiver for obtaining position and ground track; an air data sensing unit that

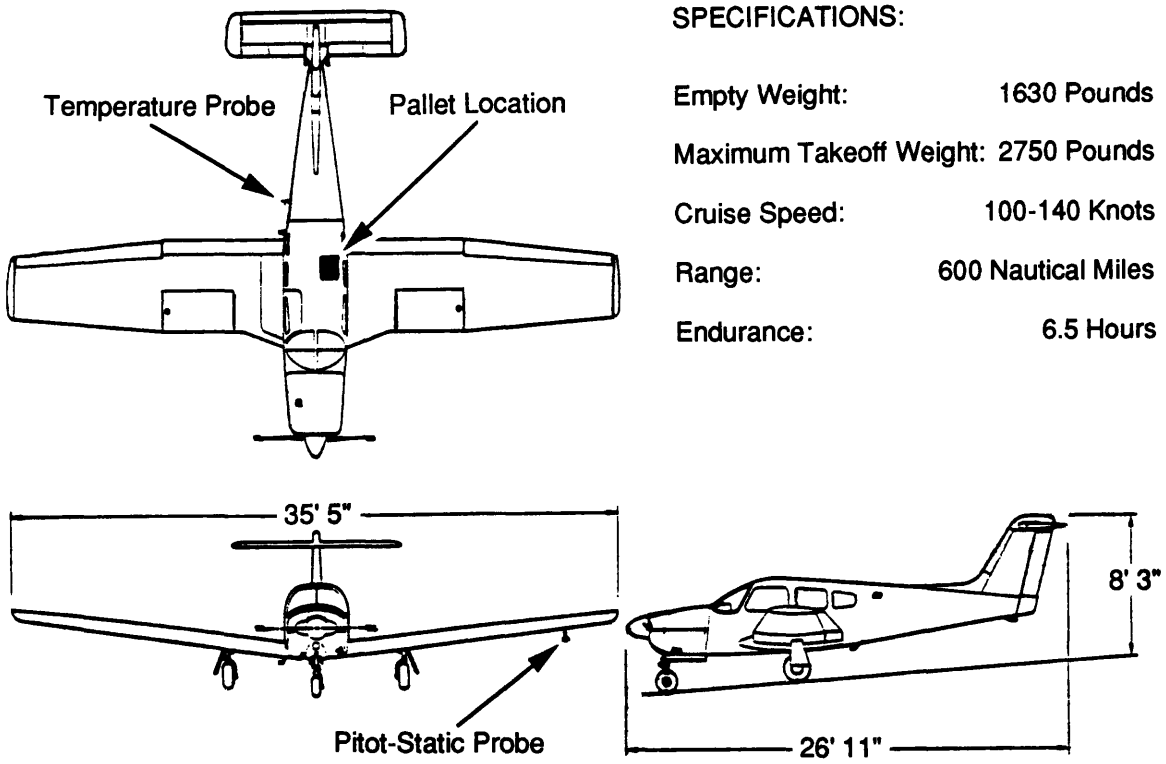

Figure 4.1 Piper Arrow IV Test Aircraft

provided altitude, airspeed, and temperature; and a directional gyro to provide magnetic heading. The air data sensing unit and directional gyro outputs were multiplexed onto one RS-232C digital serial line in an interface box, which also contained the system's electrical busses and fuses. The result was a portable system which could be quickly installed in a variety of aircraft. Airworthiness and flight test safety considerations were simplified since the pallet functioned independently of the aircraft's systems.

4.2.1 Instrumented Pallet

The instrumented pallet shown in Figure 4.3 was a two-tiered structure of aluminum and steel approximately 23" deep by 17" wide by 23" tall. A factory-made seat structure served as the pallet base and allowed the unit to slide into the left rear seat rails

after the standard seat was removed. The entire assembly was designed to withstand 12g forward and downward crash loads.

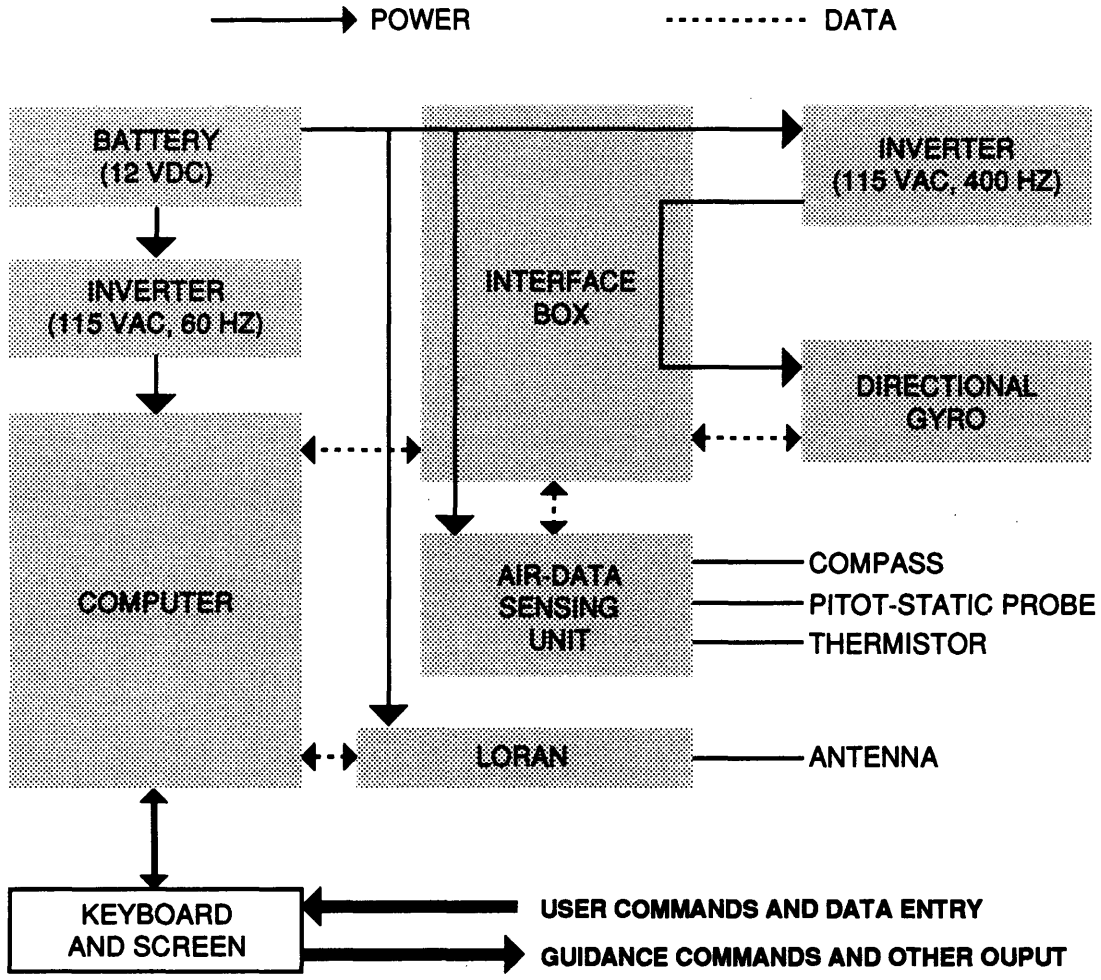

Figure 4.2 Instrumentation Schematic

A 12 volt, 80 amp-hour gel cell battery was chosen as the system power source to avoid interfacing with the airplane's electrical bus, thus reducing complexity of installation in the vehicle. This also simplified licensing requirements and minimized concerns that an equipment failure on the pallet would endanger operation of the aircraft's primary flight systems. Battery capacity was specified as six hours to allow two three-hour flight tests on each charge. A 200-watt inverter supplied the computer with 115 VAC at 60 Hz, and another inverter provided the directional gyro with 115 VAC at 400 Hz.

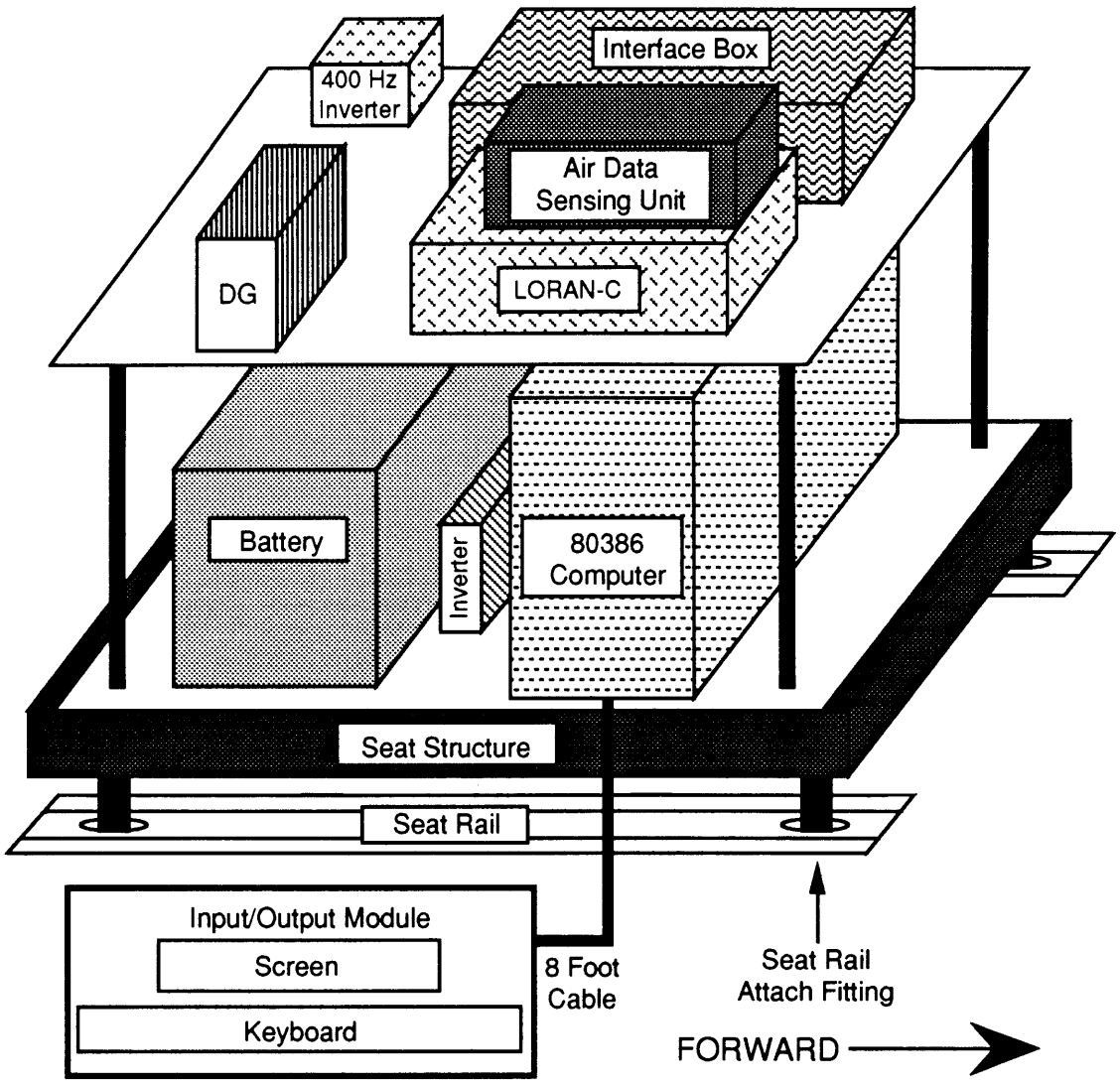

Figure 4.3 Instrumentation Pallet (wiring omitted for clarity)

4.2.2 Computer

Software was run on an IBM-PC-compatible portable computer with an 80386 CPU running at 20 MHz, 4 MB of RAM, 40 MB hard disk drive, and two RS-232C serial ports for connecting to the LORAN and interface box. The detachable screen and keyboard were mounted together and could be positioned up to eight feet from the computer permitting use by the test engineer in the front right seat of the aircraft.

The test engineer invoked strategic and tactical planning functions through the **Input/Output** window of the user interface. The computer took from 10 to 40 seconds to execute the trajectory planning algorithm. Planner output was in the form of textual commands for the pilot, who implemented changes in parameters such as power, airspeed, and altitude. The screen interface included a **Current State** window which displayed the time, current air data measurements, altimeter setting, and correction factors being applied to incoming data. All planner actions and their resulting outputs (e.g. flight plans and wind measurements) were written to a flight test history file for postflight analysis.

4.2.3 Position Sensing

Position sensing was provided by an IFR-certifiable King KLN 88 LORAN-C receiver with RS-232C outputs of latitude, longitude, groundspeed, magnetic ground track, and current signal quality. The signal quality information, in the form of station signal-to-noise ratios, enabled close control of experimental conditions. In a flight test performed to examine groundspeed vector measurement dynamics, square patterns were flown with abrupt heading changes at the corners. Postflight analysis revealed that the magnetic ground track output by the LORAN had a first-order lag of 15-25 seconds.

4.2.4 Air Data Sensing

Air data sensing was accomplished by a Cambridge Aero Instruments S-NAV, a compact (3"x3"x8") sailplane racing computer. The instrument (depicted schematically in Figure 4.4) housed pressure, temperature, and flow rate transducers, and featured a very low power consumption of 3 watts. A thermistor and pitot-static probe allowed measurement of outside air temperature, altitude, and indicated and true airspeed. Airspeed was calculated by measuring the flow through a calibrated orifice between the pitot and static pressure lines. A vertical card compass with a shaft encoder supplied magnetic heading to the S-NAV. Sensor data was sampled at 4 Hz and routed through a one-second

moving-average buffer that acted as a lowpass filter of measurement noise. Every two seconds, airspeed, altitude, temperature, and heading were sent to the interface box over an RS-232C interface.

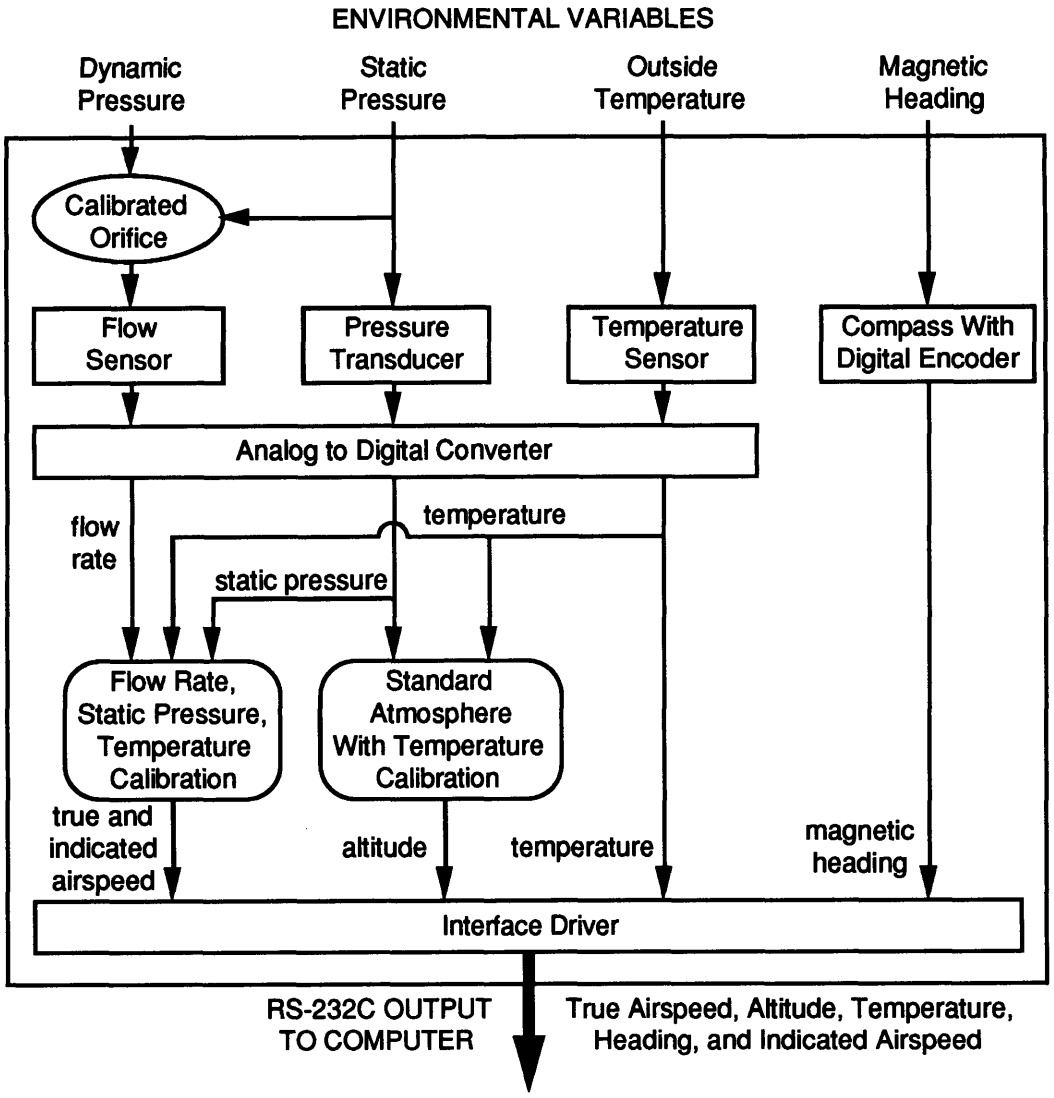

Figure 4.4 S-NAV Air Data Sensing Computer

Measurement errors were estimated by the manufacturer to be 100 feet in pressure altitude, 3-5 knots in airspeed, and several degrees in heading. Pressure altitude was corrected to indicated altitude using the local altimeter setting. S-NAV outputs were calibrated against the Arrow's flight instruments (assumed as a reference) to develop a software bias and linearity correction to sampled air data. A real-time altitude correction

factor, periodically calculated by comparing the S-NAV altitude to the aircraft altimeter, was also applied. S-NAV compass errors were often large (up to 20 degrees) and sporadic, so a directional gyroscope was added to the sensing package for accurate heading information.

4.2.5 Directional Gyroscope

Magnetic heading was supplied by a King KSG-105 electrically-driven directional gyro (DG) system. The gyro was occasionally slaved (in the same way a panel-mounted DG is reset during flight) to the aircraft compass. The DG heading was output in a five-wire synchro format with an internally-generated 26 VAC, 400 Hz excitation signal. A conversion circuit housed in the interface box translated the synchro signal into an RS-232C format.

4.2.6 Sampling Procedure

Every 10 seconds, all air data parameters were sampled and written to a data logging file on disk. Any information in the data stream could be modified to satisfy experimental needs. For example, the sensor signals could be corrupted by a controlled noise signal to simulate difficult measurement situations.

4.3 Wind and Temperature Measurements

Measurements of the local wind vector **W** were based on the relationship of vector groundspeed **GS** to vector true airspeed **TAS**:

$$\mathbf{GS} = \mathbf{TAS} + \mathbf{W} \tag{4.1}$$

$$\mathbf{W} = \mathbf{GS} - \mathbf{TAS} \tag{4.2}$$

The groundspeed vector was output by the LORAN receiver as groundspeed and magnetic ground track. Temperature and true airspeed magnitude were supplied by the S-NAV, and

true airspeed direction was the magnetic aircraft heading measured with the DG. A 50-second moving-average window was employed in making wind and temperature measurements to reject unwanted high-frequency process noise.

5 Strategic Planning Tests

This chapter details flight tests performed to investigate strategic trajectory planner performance using the fused-sensor wind model. Test results are discussed along with suggested improvements to the air data acquisition system.

5.1 Procedure

Four traversals were made on the 55-nm great-circle route between Bedford, Massachusetts and Turners Falls, Massachusetts (shown on Figure 5.1). The test

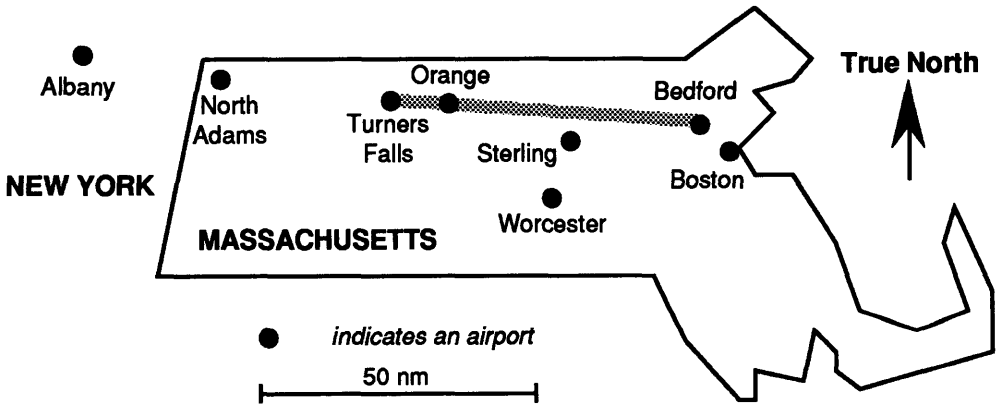

Figure 5.1 Flight Test Region

engineer performed the mission management function by initiating planning of minimum-time altitude profiles. On two of the flights the wind and temperature model was initialized with a forecast numerically generated by the National Weather Service and obtained from an FAA Flight Service Station. On the other two, an intentionally-

flawed "bad" forecast was used to investigate the system's response to erroneous forecast information. The test matrix was as follows:

Table 5.1 Trajectory Planner Flight Test Matrix

Test Number	Origin Airport	Destination Airport	Ground Track	Forecast Type
1	Bedford	Turners Falls	279°	Good
2	Turners Falls	Bedford	99°	Good
3	Bedford	Turners Falls	279°	Bad
4	Turners Falls	Bedford	99°	Bad

All four tests were done on December 18th, 1992 between 1:30 PM and 4:00 PM Eastern Standard Time to minimize changes in meteorological conditions from test to test. To begin Test 1, the aircraft departed Hanscom Field in Bedford and flew to Turners Falls where an approach and runway flyover were executed. A turnaround was performed in the air while the system was configured for the next test, which was commenced with a runway flyover at Turners Falls. This turnaround procedure was completed again at Bedford and once more at Turners Falls before the last test ended in a landing at Bedford.

5.2 Winds Aloft Forecasts

The winds aloft forecast for the flight test called for strong northeasterly winds increasing with altitude over the flight test region. Measured conditions were consistent with the forecast, with windspeeds as great as 58 knots from 339 degrees measured near an altitude of 6500 feet. The winds aloft forecasts obtained for the Boston, Massachusetts and Albany, New York reporting stations are shown in Tables 5.2 and 5.3.

Table 5.2 Winds Aloft Forecast at Boston, Massachusetts (valid from 1 PM to midnight Eastern Standard Time)

Altitude [feet]	Wind Direction [degrees true]	Wind Speed [knots]
3000	340	29
6000	330	29
9000	300	38
12000	290	51

Table 5.3 Winds Aloft Forecast at Albany, New York (valid from 1 PM to midnight Eastern Standard Time)

Altitude [feet]	Wind Direction [degrees true]	Wind Speed [knots]
3000	350	18
6000	320	23
9000	300	31
12000	290	46

Figure 5.2 graphically depicts "good" forecast profiles* at Bedford and Turners Falls estimated by the wind model, which was initialized with the forecast data in Tables 5.2 and 5.3.

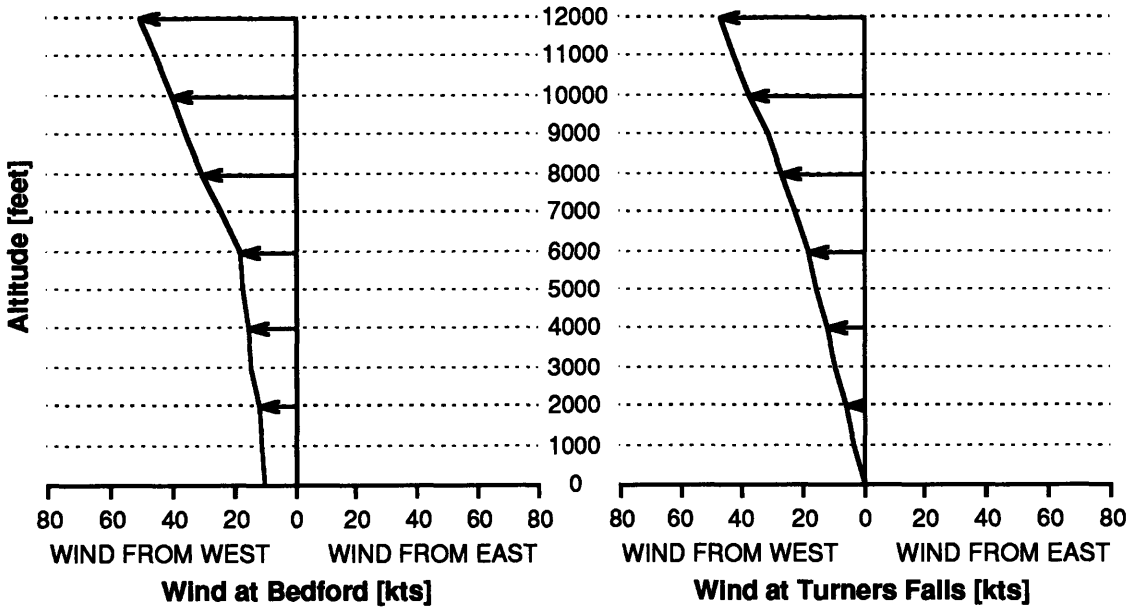

Figure 5.2 "Good" Wind Forecast Profile used for Trajectory Planner Tests

* Throughout this chapter, winds aloft profiles are presented graphically as the component of wind along the flight direction (the true course from Bedford to Turners Falls is 279°). To provide the reader with a familiar geographical reference, wind profile graphs are labeled with the captions "WIND FROM WEST" (meaning "from 279°") and "WIND FROM EAST" (meaning "from 99°"). Bedford is always shown on the left of the page - with Turners Falls on the right - to maintain a constant geographical orientation.

For tests of the planner's response to an incorrect initial wind forecast, it was desired to construct a wind profile with features significantly different from the actual profile. This was expected to cause flight plans initially generated using the bad forecast to be very different in nature from those generated using the good forecast. A profile of strong winds from the east increasing with altitude was used and is shown graphically in Figure 5.3.

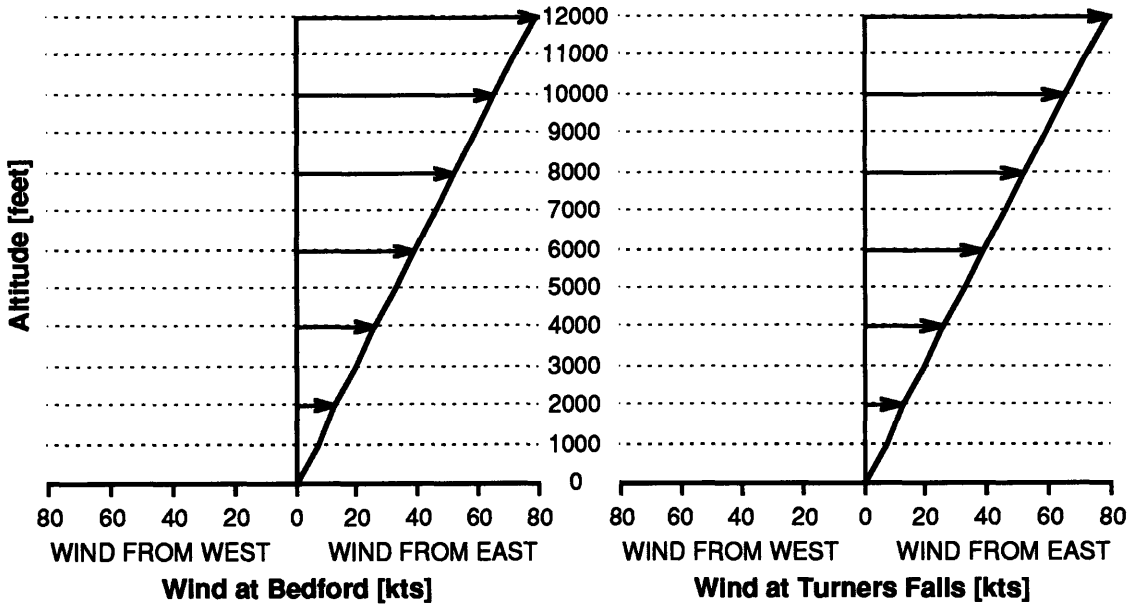

Figure 5.3 "Bad" Wind Forecast Profile used for Trajectory Planner Tests

In general, when the wind model called for headwinds, the flight plan was at the lowest altitudes compatible with terrain clearance requirements. Tailwinds increasing with altitude caused the planner to generate a high altitude profile to take advantage of the winds. The details of the four test runs are described below.

5.3 Test 1: Bedford to Turners Falls - Good Wind Forecast

An overview of the first test is shown in Figure 5.4 with terrain, the actual flight profile, points where wind and temperature measurements were taken, and locations where strategic flight plans were made. The flight proceeds from left to right across the page. A total of six flight plans were generated, including one made before takeoff from

Bedford. Four measurements were taken along the route to update the wind and temperature model. Note that the altitude axis is marked only with the altitudes available for westbound VFR flight.

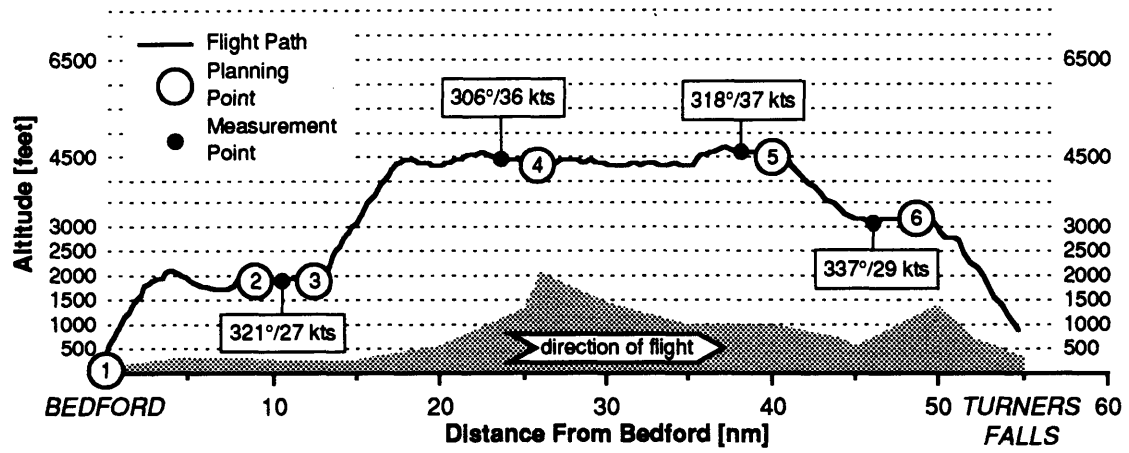

Figure 5.4 Test 1 - Overview

Measured winds were from the west, but at speeds slightly higher than predicted in the forecast. This can be seen by comparing the wind model before any measurements were made (Figure 5.5) to the estimated profiles at Bedford and Turners Falls after three measurements had been made (Figure 5.6):

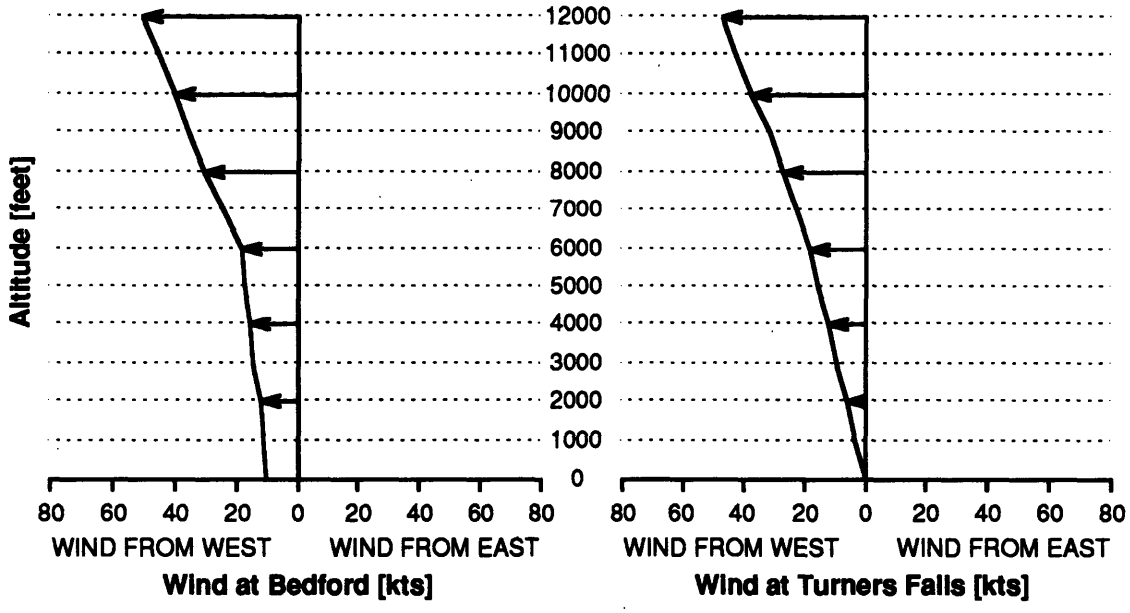

Figure 5.5 Test 1 - "Good" Initial Wind Forecast Profile

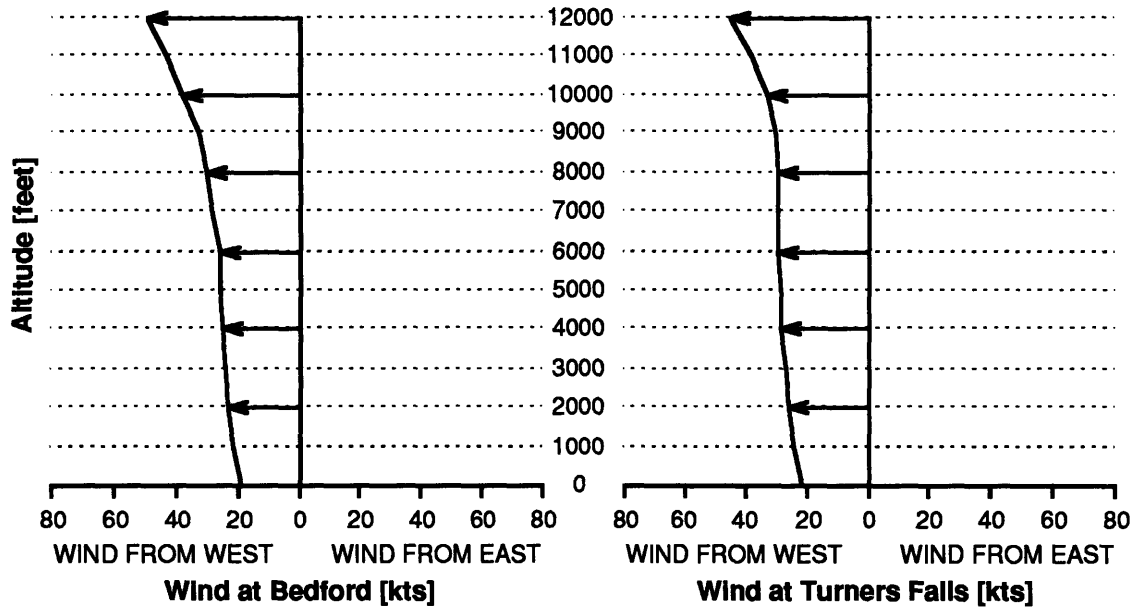

Figure 5.6 Test 1 - Estimated Wind Profile After Three Measurements

The next sequence of figures depicts the flight plans generated at successive points along the flight path. The first two plans (shown in Figures 5.7 and 5.8) were of the low-altitude type. These plans proceeded at 2000' until requiring a climb to 3000' for terrain clearance midway through the test.

The first two plans assumed a headwind gradient that outweighed the rise in true airspeed with altitude predicted by the performance model; it was best to fly as low as possible. By the third planning point however, the wind model had changed to reflect the first wind measurement. The planner wind model changed during the test so that the headwinds at low altitudes were stronger than initially expected; the profile was almost flat for altitudes between 3000' and 6000'. The flat wind profile used to generate the third plan allowed the true airspeed rise with altitude to come into play; instead of flying at 3000', the third plan used a 4500' cruising altitude. It was now worthwhile to climb 1500' more for a slight increase in true airspeed. The fourth plan generated was the same as the third because the second wind measurement did not change the wind estimate enough to alter the flight plan.

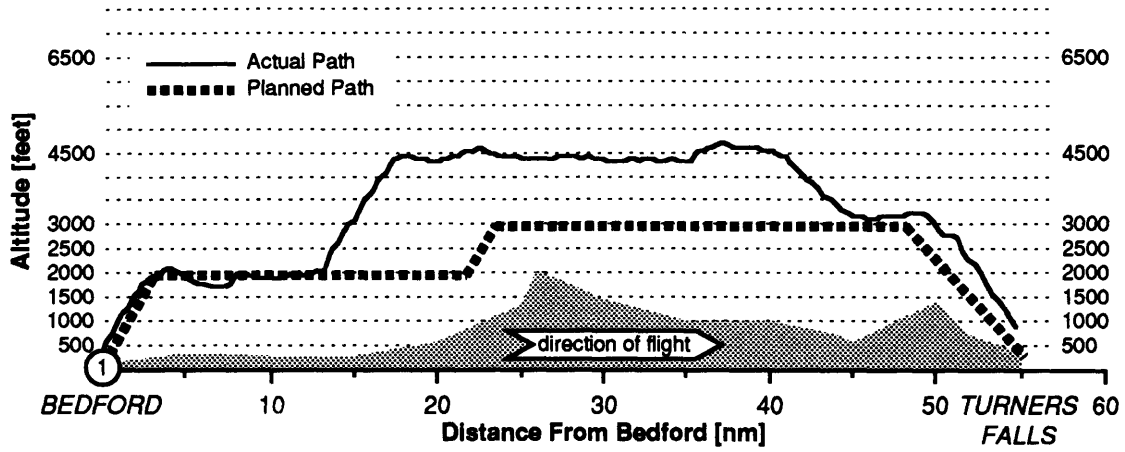

Figure 5.7 Test 1 - Flight Plan 1

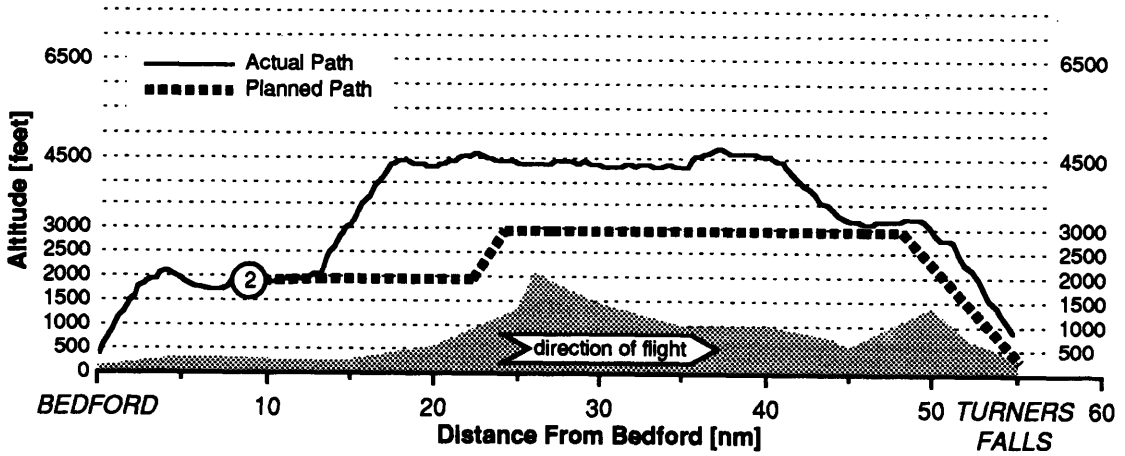

Figure 5.8 Test 1 - Flight Plan 2

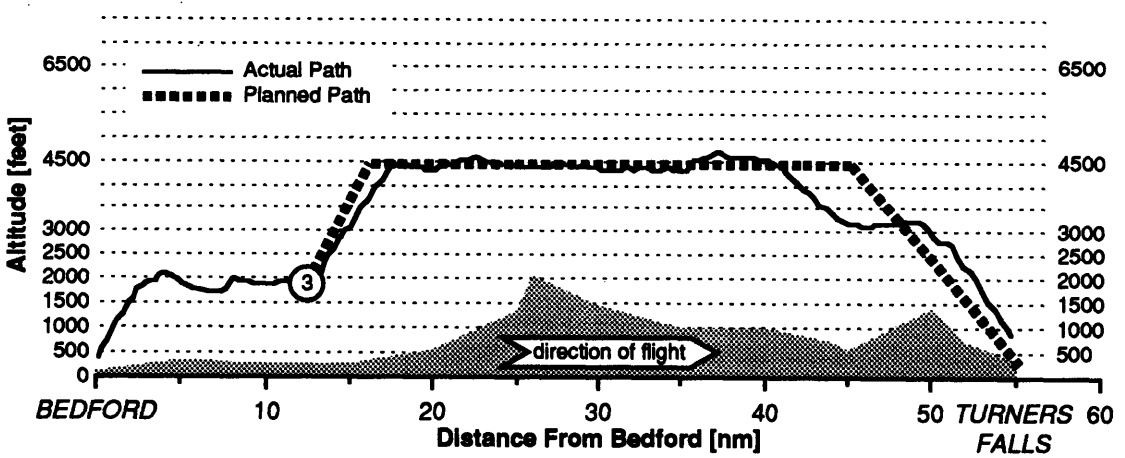

Figure 5.9 Test 1 - Flight Plan 3

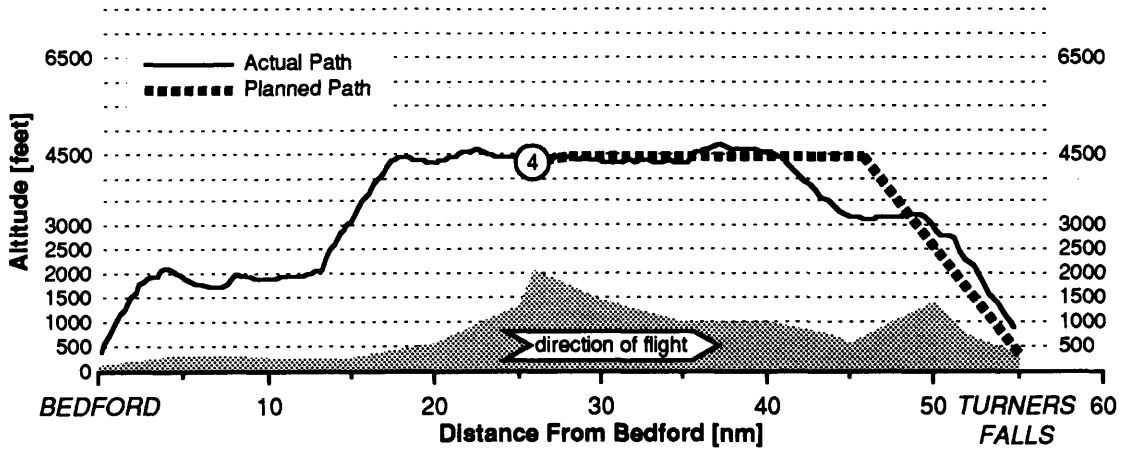

Figure 5.10 Test 1 - Flight Plan 4

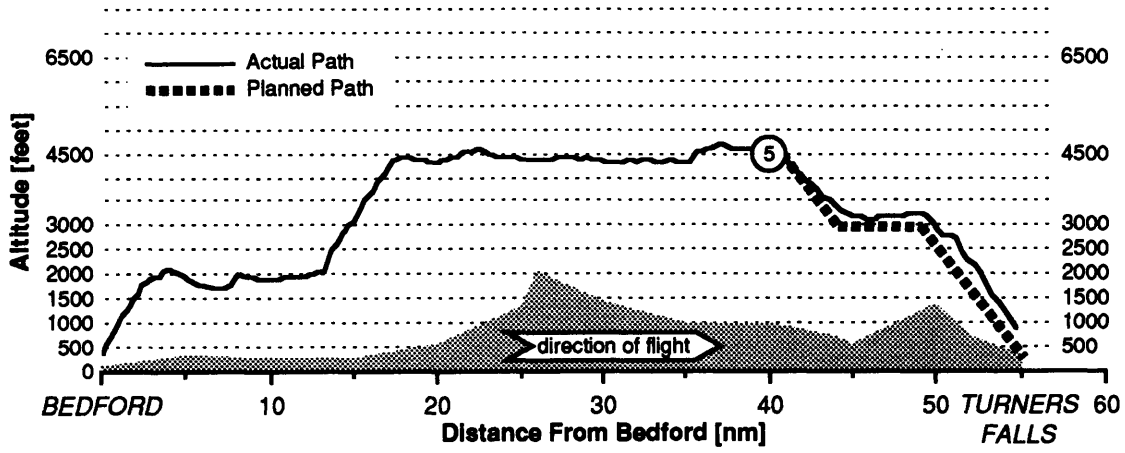

Figure 5.11 Test 1 - Flight Plan 5

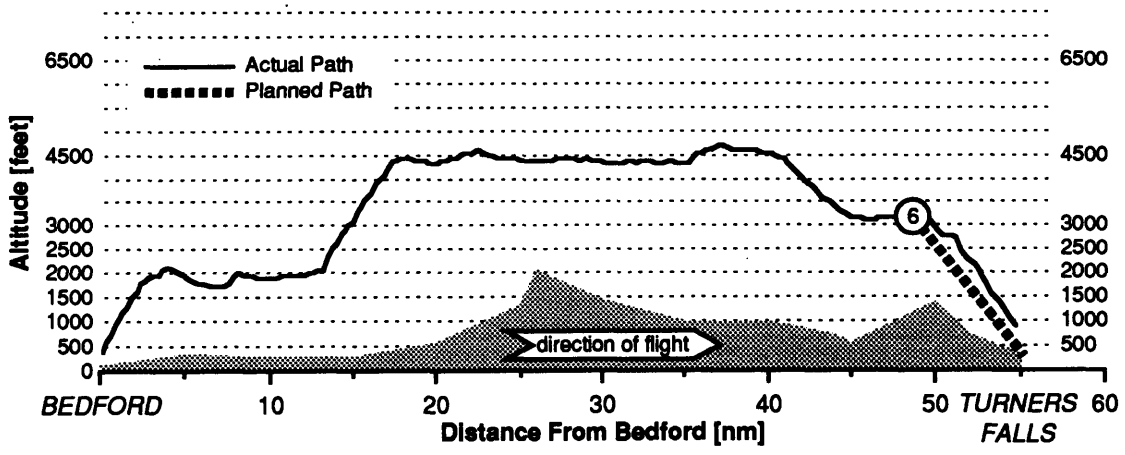

Figure 5.12 Test 1 - Flight Plan 6

The fifth plan (shown in Figure 5.11) separated the descent into two stages: one to 3000', and then finally to Turners Falls airport. This small change in the plan was due to fusion of the wind measurement taken approximately 38 nm from Bedford. By the time the sixth plan was generated (see Figure 5.12), the aircraft was so close to the destination that the planner had no other options than to plan an immediate descent.

5.4 Test 2: Turners Falls to Bedford - Good Wind Forecast

While the aircraft was completing the approach and turnaround maneuver west of Turners Falls, the system was reconfigured with the original "good" wind forecast with no measurements so that the initial plan would be based on the same model as the initial plan made during the first test. Figure 5.13 overviews this test and depicts the four measurement points and four planning points during the test, which moves from right to left on the page.

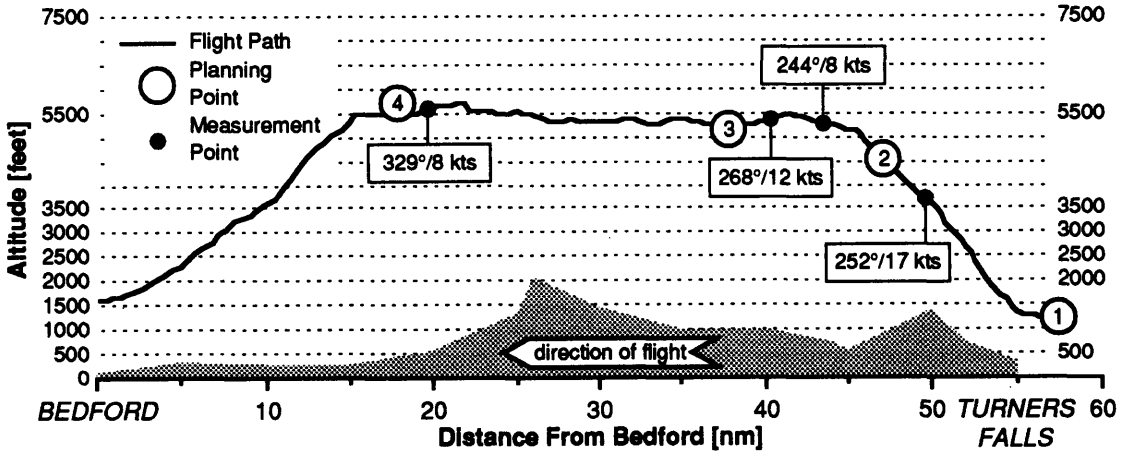

Figure 5.13 Test 2 - Overview

Measurements taken on the route back to Bedford indicated smaller windspeeds from the west than those measured during Test 1. This pattern, which continued over all the tests, suggests a systematic error in one of the sensors used to make wind measurements. This apparent bias is discussed later in this chapter. As a result, the estimated wind profile at the end of Test 2 (Figure 5.14) shows lighter winds coming

from the west, compared to the estimated profile at the end of the first test (Figure 5.6). For example, a 10 kt wind was estimated at 6000' on the flight to Bedford, while a 25 kt wind had been estimated at 6000' on the initial flight to Turners Falls.

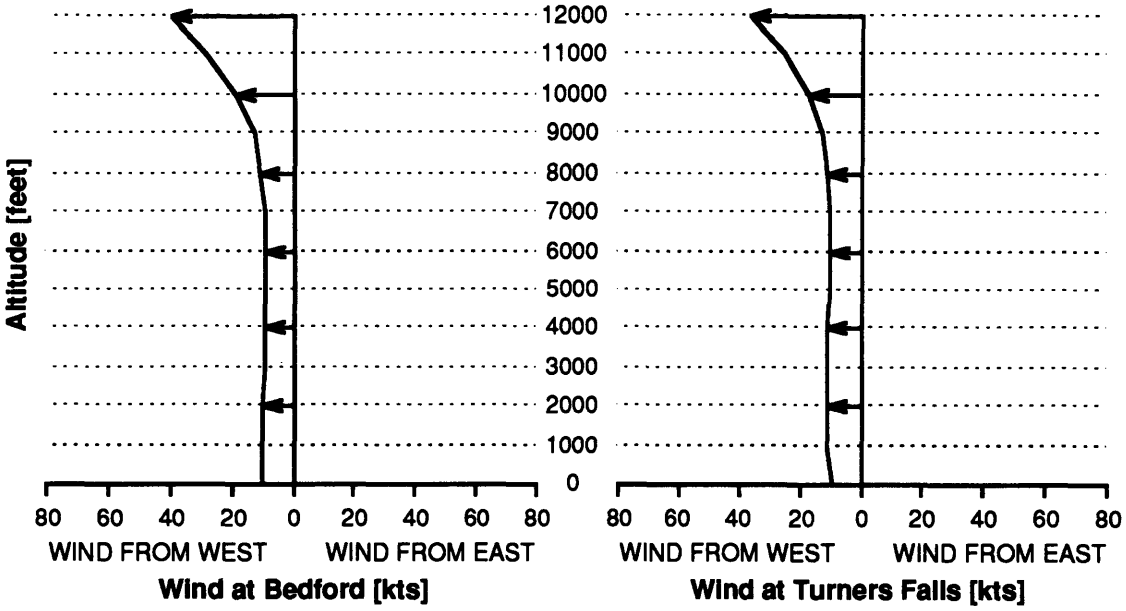

Figure 5.14 Test 2 - Estimated Wind Profile After Four Measurements

Since the forecast was for tailwinds from the west increasing with altitude, the initial plan (Figure 5.15) was to climb directly to a cruise altitude of 7500' and remain there until the end of the test. This cruise altitude was a balance between the wind profile, the aircraft's true airspeed versus altitude curve, and the length of the flight.

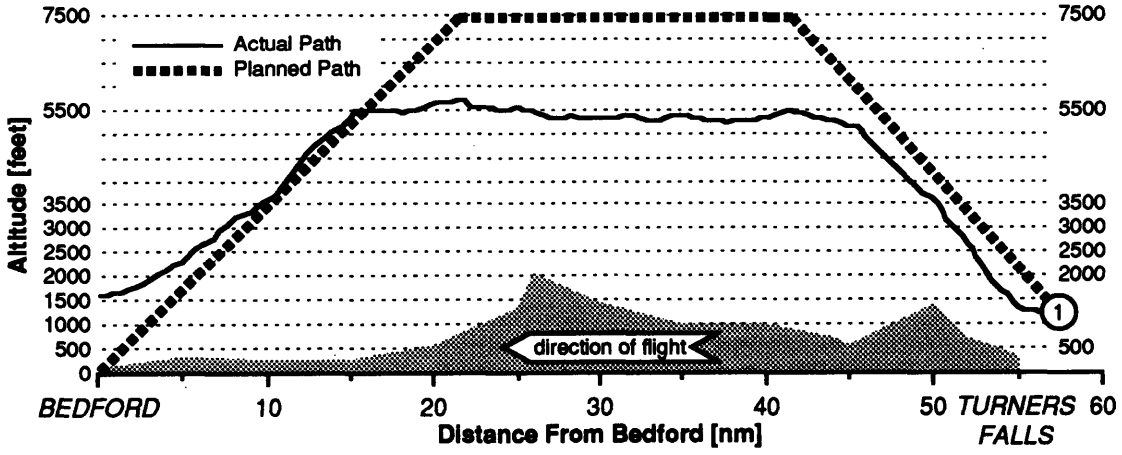

Figure 5.15 Test 2 - Flight Plan 1

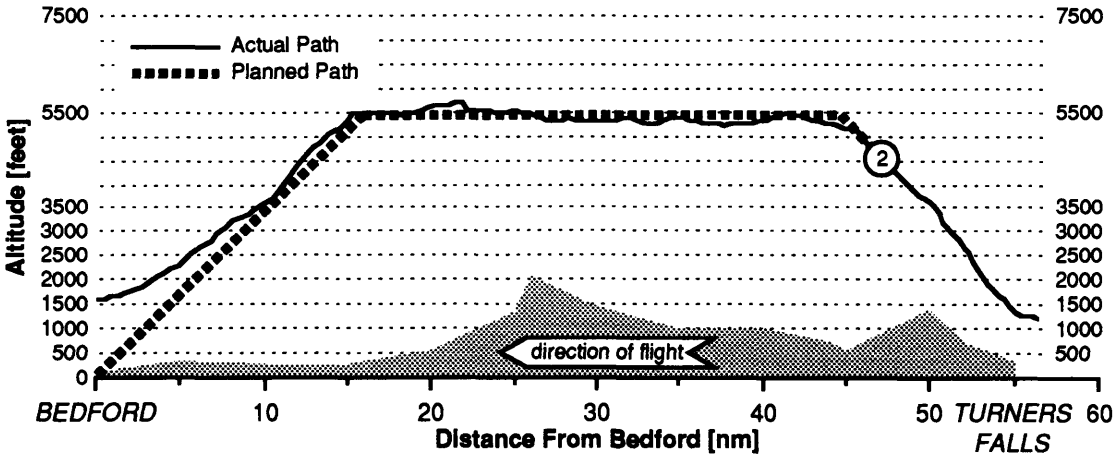

Figure 5.16 Test 2 - Flight Plan 2

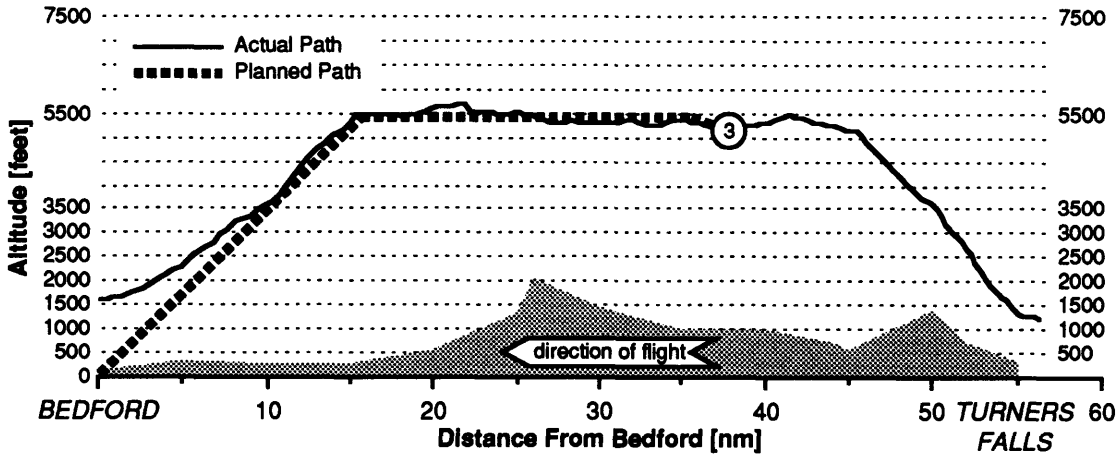

Figure 5.17 Test 2 - Flight Plan 3

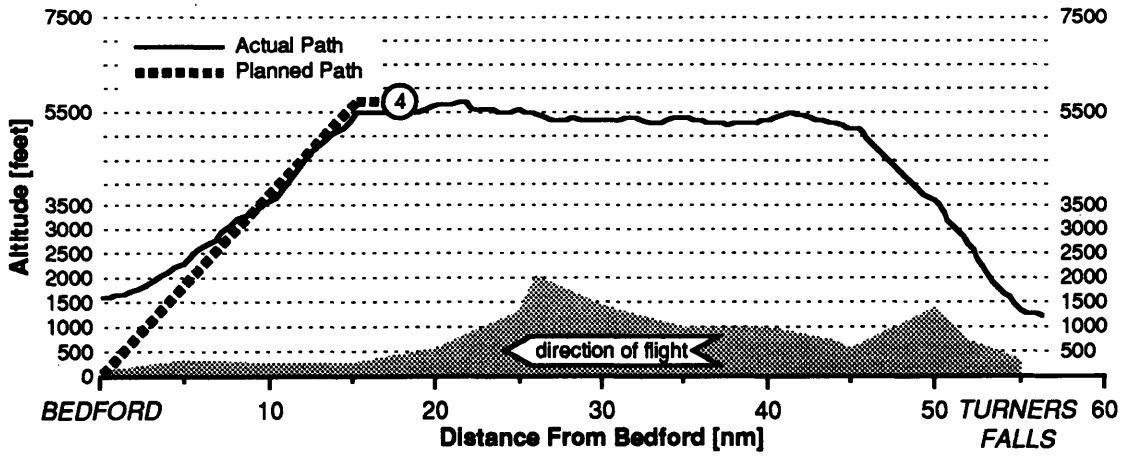

Figure 5.18 Test 2 - Flight Plan 4

Figures 5.16 through 5.18 show the remaining plans generated during Test 2. By the time the second plan was generated the estimated tailwinds were not as large as forecast, so it was not worthwhile to climb all the way to 7500'. The second plan, shown in Figure 5.16, has a cruise altitude of 5500', as do the third and fourth plans. This test ended with an overflight of Hanscom Field in Bedford.

5.5 Test 3: Bedford to Turners Falls - Bad Wind Forecast

A turnaround was made to the northeast of Bedford where the "bad" wind forecast was loaded and an initial plan was generated for the flight to Turners Falls. This test is overviewed (proceeding from left to right) in Figure 5.19.

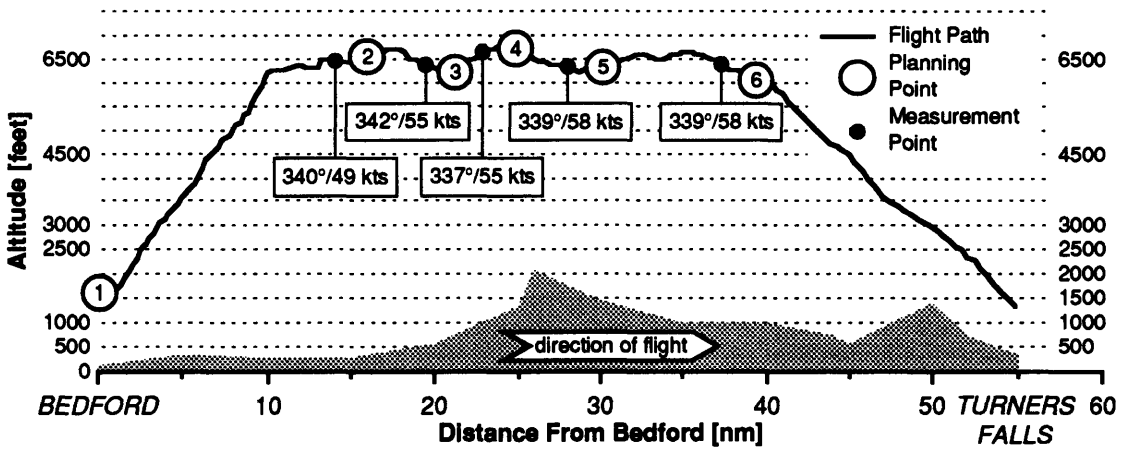

Figure 5.19 Test 3 - Overview

The evolution of the wind model during this test provides a good example of sensor fusion effects and will be described in detail here. Figures 5.20 through 5.25 show the progressive development of the estimated wind profile as the five measurements made during the test were fused into the model. Figure 5.20 shows the "bad" forecast profile before any wind measurements were incorporated. The first measurement had a large impact, turning the estimated winds at 8000' and below from tailwinds into headwinds (see Figure 5.21). Each additional measurement provided additional weighting in favor of a headwind profile. Figure 5.25, the estimated profile after all five measurements had

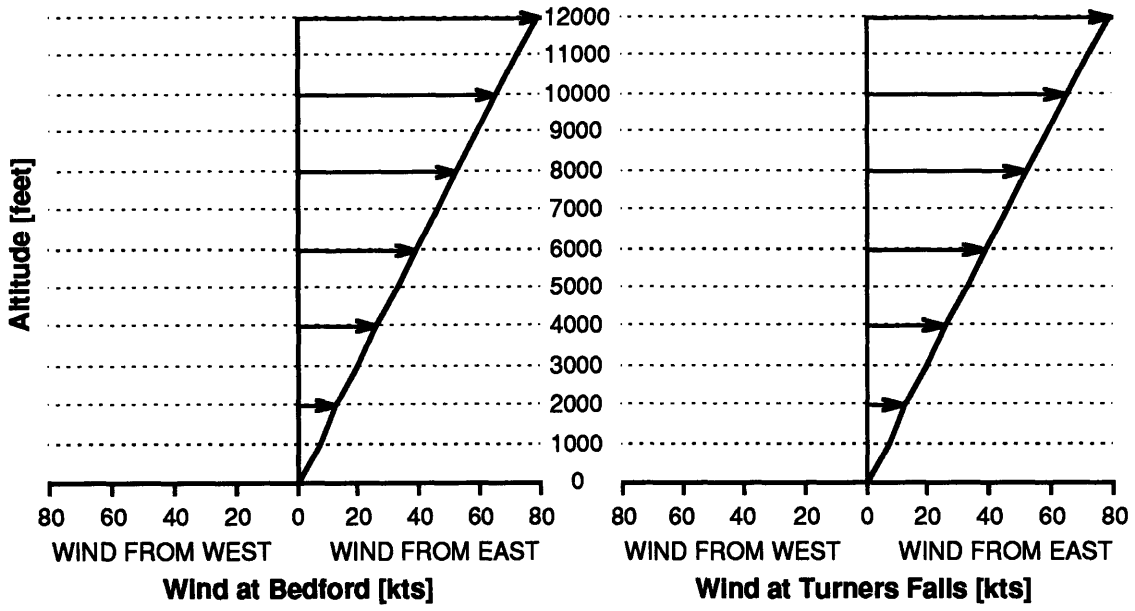

Figure 5.20 Test 3 - "Bad" Initial Wind Forecast Profile

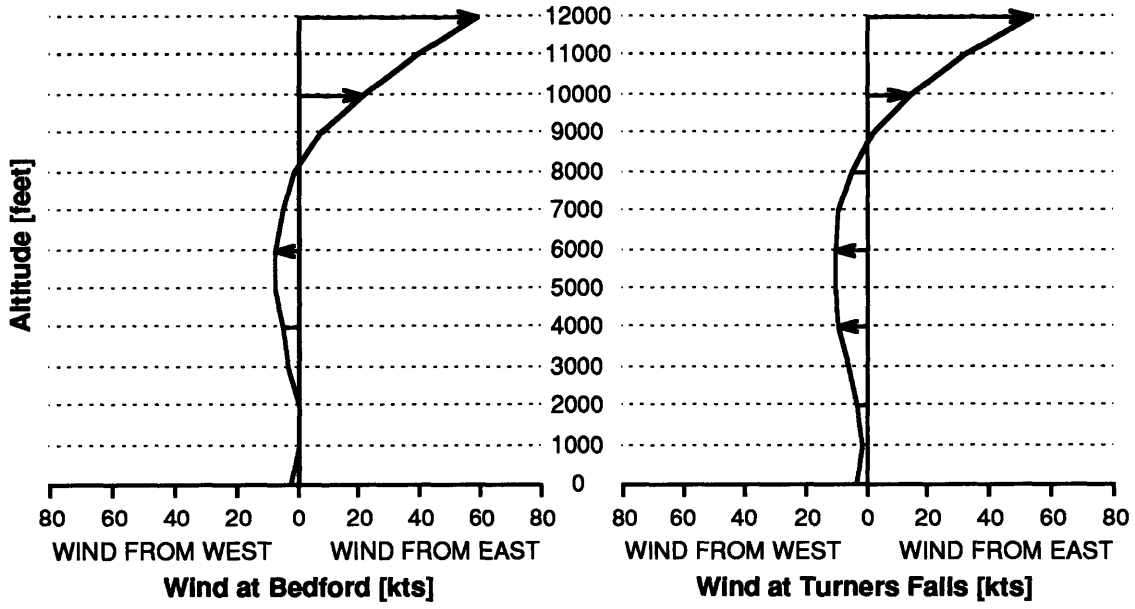

Figure 5.21 Test 3 - Estimated Wind Profile After One Measurement

been fused, looks very similar to the final profile attained on the Test 1 using a good forecast; both profiles show winds from the west in the 30 knot range up to about 8000'. In other words, the wind model had successfully used wind measurements to correct its grossly-inaccurate forecast information and recovered the information modeled during the first test, which used an accurate forecast.

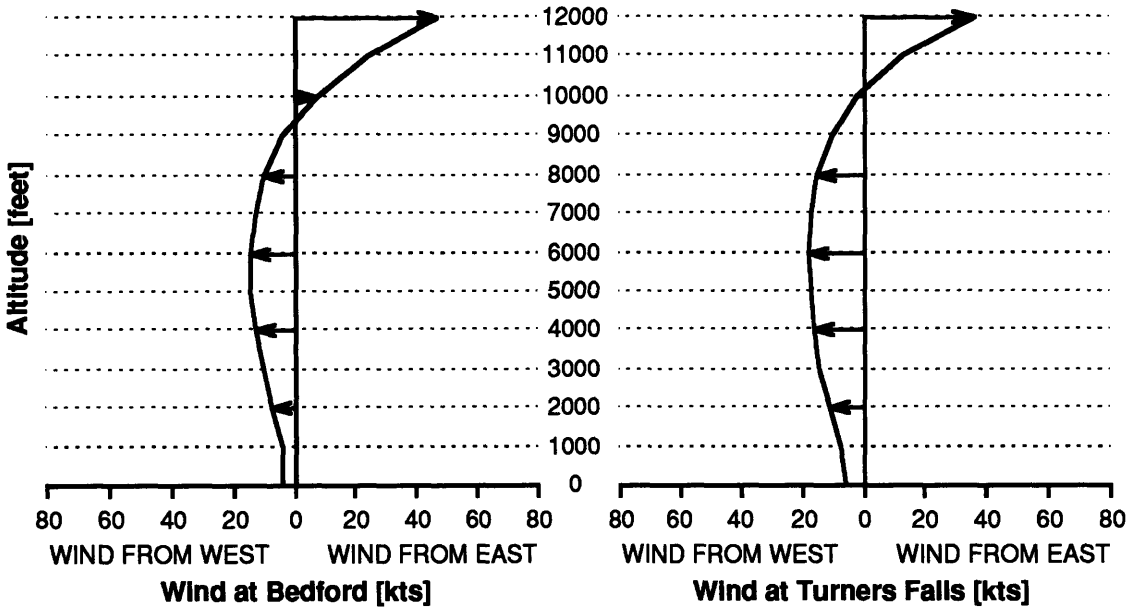

Figure 5.22 Test 3 - Estimated Wind Profile After Two Measurements

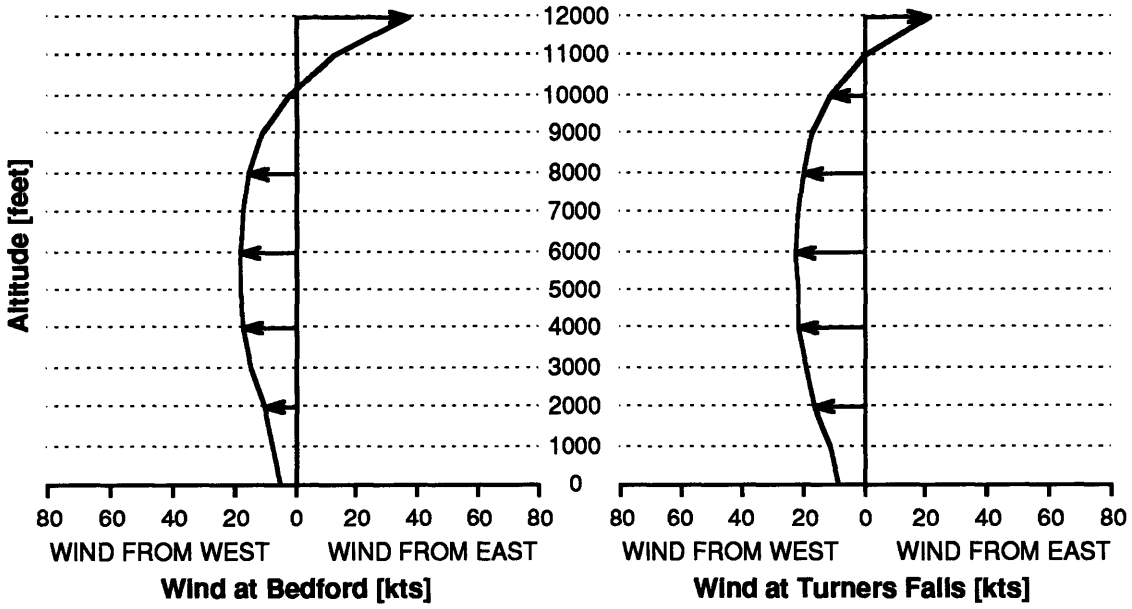

Figure 5.23 Test 3 - Estimated Wind Profile After Three Measurements

Note that above 8000' the final estimated profiles for Tests 1 and 3 diverge. This is because for both the good and bad forecast cases, both profiles rely primarily on forecast information for altitudes above 8000'. Since the aircraft never climbed above 7500' on any of the tests, no wind measurements were made above this altitude. While similar measurements caused similar low-altitude wind profiles, the "good" forecast case

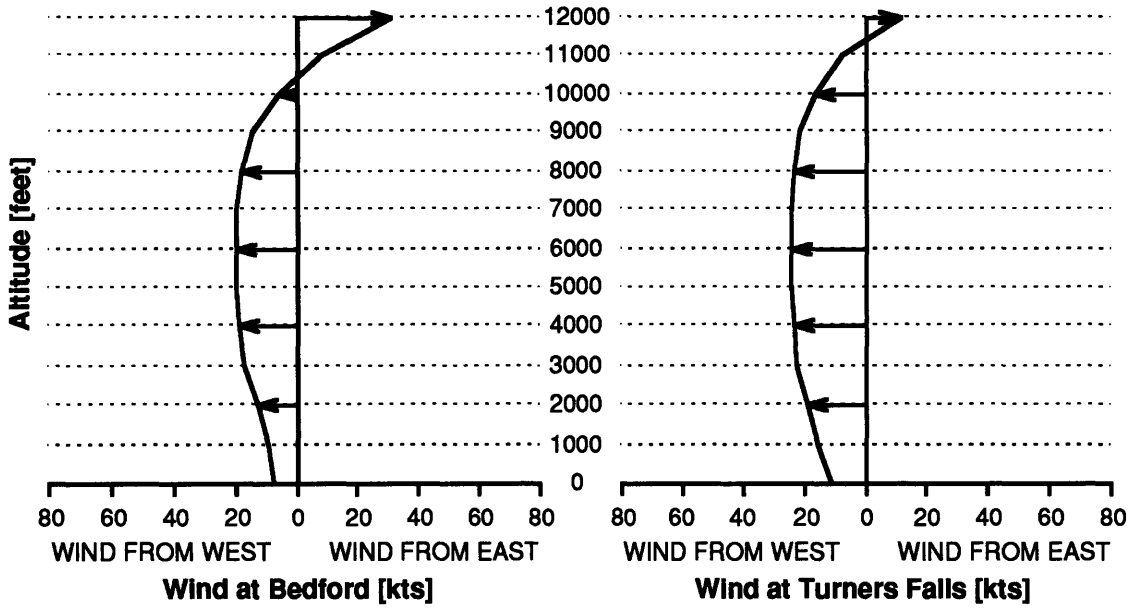

Figure 5.24 Test 3 - Estimated Wind Profile After Four Measurements

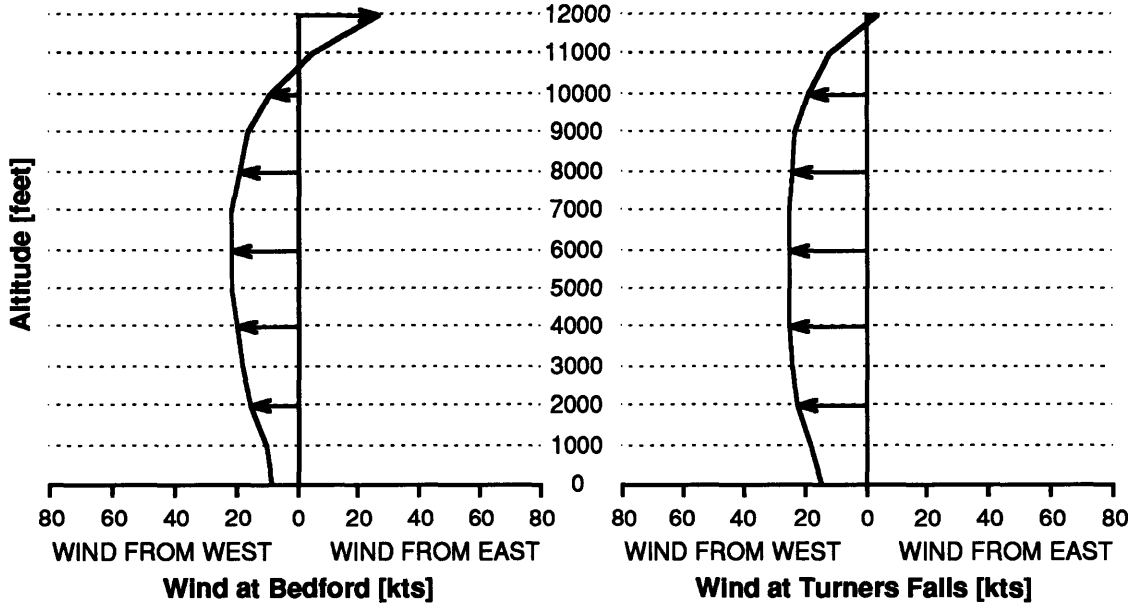

Figure 5.25 Test 3 - Estimated Wind Profile After Five Measurements

shows 50 knot winds from the west at 12000', while the "bad" forecast case predicts little wind at all. This disparity is obviously dependent on the value of σ_{vm} used by the wind model's altitude weighting function. A larger value of σ_{vm} would have spread the influence of measured data to higher altitudes - at the expense of loss of detail in the estimated wind profile.

Figure 5.26 shows the first plan generated using the "bad" wind model. Since the corrupted forecast predicted tailwinds, this initial plan was of the high-altitude type with a cruise altitude of 6500'. The aircraft was climbed to 6500' where the first measurement

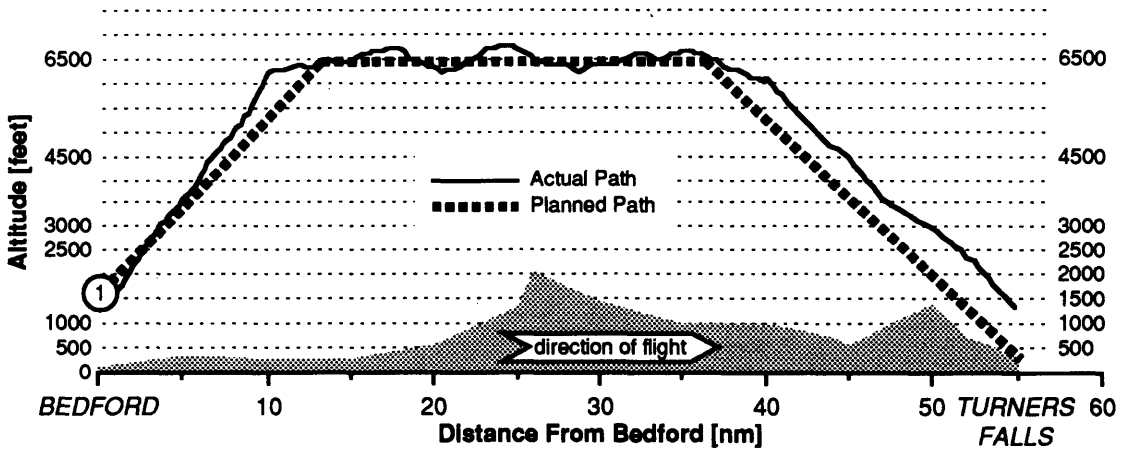

Figure 5.26 Test 3 - Flight Plan 1

was taken. Even though the estimated wind profile rapidly changed to reflect that there were headwinds and not tailwinds, the second and all subsequent plans had cruise altitudes of 6500'. The second and fifth plans are shown in Figures 5.27 and 5.28. One might have expected the planner to generate low-altitude plans after making headwind measurements. Several reasons contributed to the unchanged cruise altitude of 6500'. First, the modeled wind profile after integrating measurements (Figures 5.21 through 5.25) was relatively flat in the altitude range from 2000' to 8000'. Second, higher

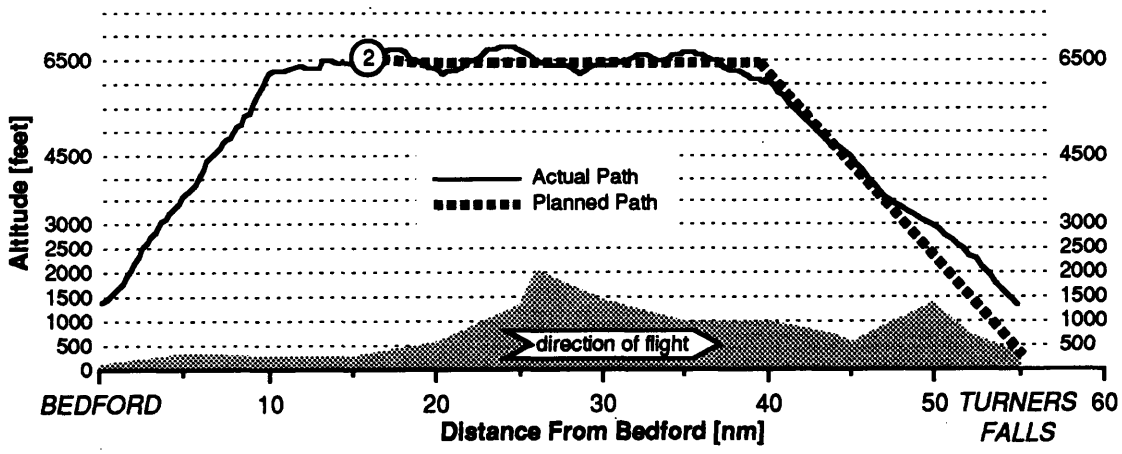

Figure 5.27 Test 3 - Flight Plan 2

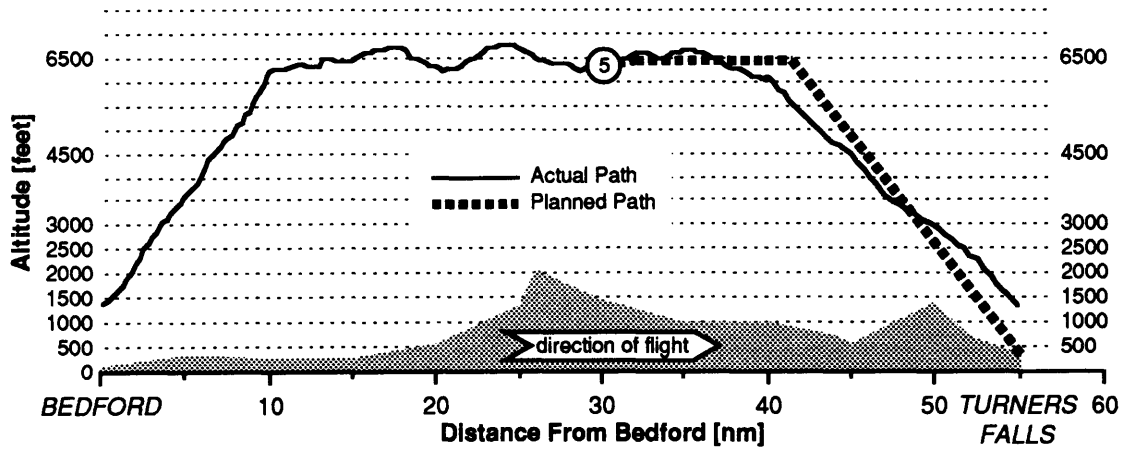

Figure 5.28 Test 3 - Flight Plan 5

altitudes were favored by the aircraft model's true airspeed increase with altitude. Finally, the time savings that might have been gained by descending earlier were outweighed by the extra 12-second altitude transition penalty incurred by adding an extra descent arc.

5.6 Test 4: Turners Falls to Bedford - Bad Wind Forecast

After a turnaround and reloading of the bad wind forecast, the final test (overviewed from right to left in Figure 5.29) was commenced with an overflight of Turners Falls airport.

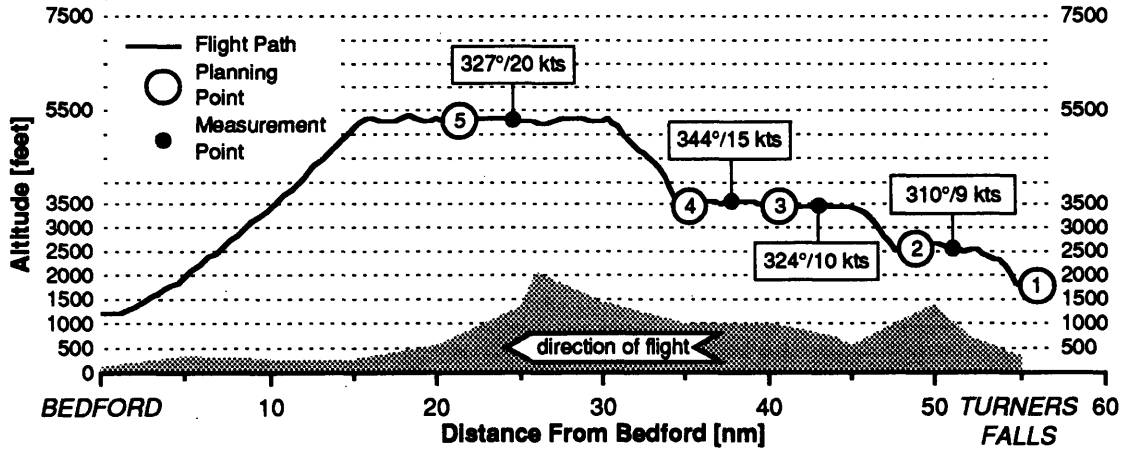

Figure 5.29 Test 4 - Overview

Once again, the system rapidly learned from measurements that winds were from the west, not the east as predicted by the bad forecast. The final estimated wind profile, shown in Figure 5.30, shows a small wind from the west at altitudes below 6000'. Above 7000' there is still an easterly wind increasing with altitude since the aircraft never took measurements above 5500'. Again it is important to note that the measured westerly winds during the fourth test were consistently smaller than those measured less than a half-hour earlier during Test 3, strongly suggesting a measurement bias.

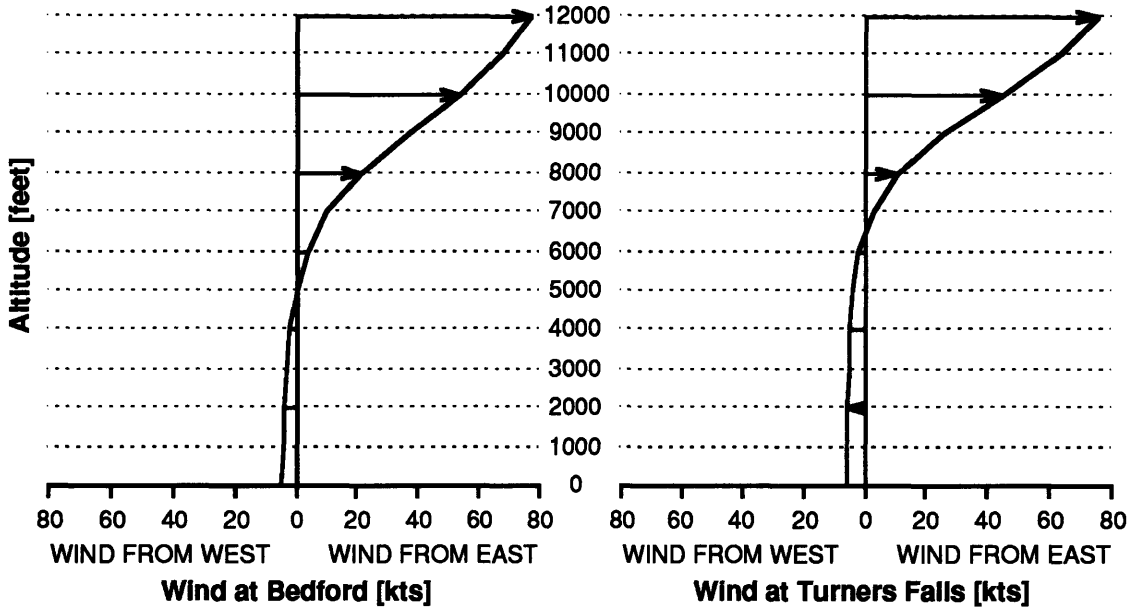

Figure 5.30 Test 4 - Estimated Wind Profile After Three Measurements

The initial plan, shown in Figure 5.31, was of the terrain-following type, since the planner expected headwinds increasing with altitude. The plan first followed the terrain contour at 2500', then climbed to 3000' to clear terrain midway between Turners Falls and Bedford. The last segment of the plan was at 1500', the lowest altitude not in the terrain exclusion zone.

The progression of flight plans reflects the system's discovery that strong headwinds were not present. The second and third plans (Figure 5.32 shows the second plan) had a constant cruise altitude of 3500', with no climbs or descents for terrain

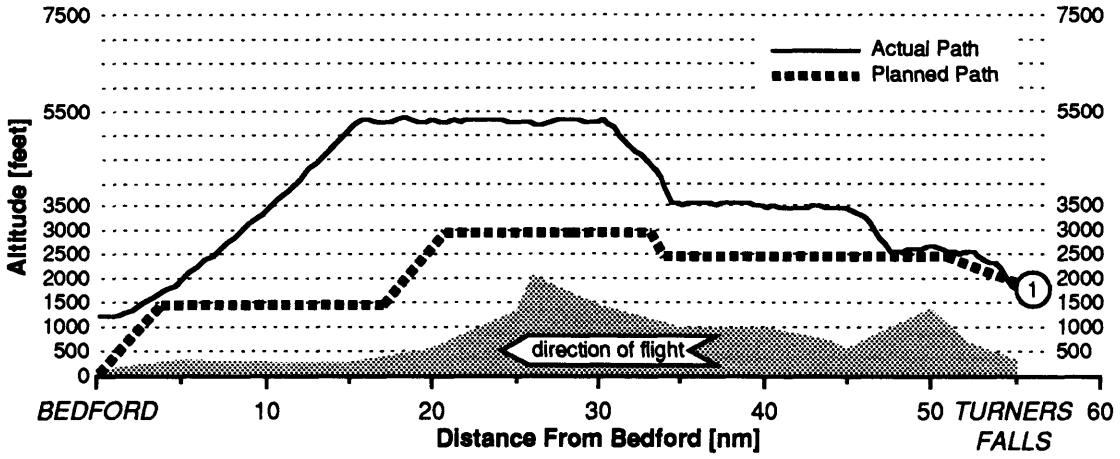

Figure 5.31 Test 4 - Flight Plan 1

following. The fourth and fifth plans (the fourth plan is shown in Figure 5.33) had a higher cruise altitude to take advantage of the aircraft's higher true airspeed at 5500'.

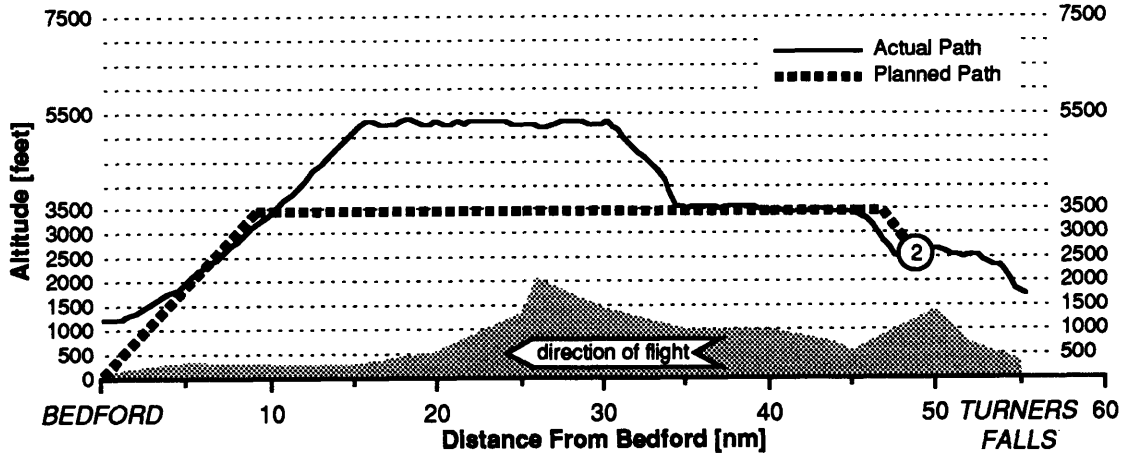

Figure 5.32 Test 4 - Flight Plan 2

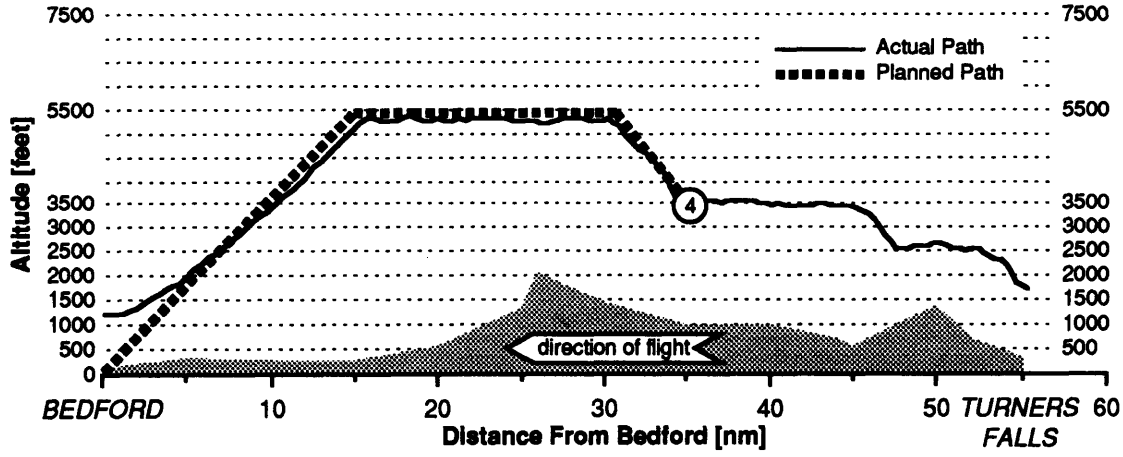

Figure 5.33 Test 4 - Flight Plan 4

5.7 Discussion

5.7.1 Strategic Planner Performance

This demonstration of the strategic planner and dynamic wind model was successful, showing that an operational system can produce flight plans consistent with changing conditions. The wind model responded in a reasonable and stable way to sensor measurements when initialized with real and intentionally flawed forecast information. The plans generated were flyable and conformed to atmospheric and aircraft performance characteristics.

The relative insensitivity to altitude of the test aircraft's performance led the planner to produce fairly predictable flight plans for the wind profiles encountered. Headwinds produced low-altitude plans that tended to follow the contours of the terrain along the route. Tailwinds tended to produce plans with one cruise altitude dependent on the strength of the winds and affected by the length of the flight. Various scenarios would lead to more complex flight plans. Windfields with significant horizontal variations could yield plans with significantly different altitudes along the route. Examples include frontal regions, or windfields over routes long enough to span one or more weather systems. The planning problem would also change significantly for jet aircraft with their large performance variations with altitude. Plans would be highly dependent on aircraft weight, fuel burn, engine performance, and atmospheric features such as jet stream location and temperature profiles.

5.7.2 Wind Measurement Errors

Measurements made on westbound and eastbound headings appeared to exhibit systematic errors dependent on the direction of flight. As a very coarse indicator of this disparity, the average of windspeeds measured at 4500' and 6500' on the tests from Bedford to Turners Falls was 49 knots, while measurements made flying from Turners

Falls to Bedford at 5500' averaged 12 knots. Since all measurements were made during a period of two and a half hours, there is strong evidence that the difference in measurements was caused by a sensor bias. This postulated measurement bias is reflected in the profiles estimated by the fused-sensor wind model. For example, the estimated wind profile at the end of Test 1 (repeated as Figure 5.34) indicates stronger winds from the west than the profile estimated at the end of Test 2 (repeated as Figure 5.35). Through the complex chain of measurement, sensor fusion, and trajectory generation, instrumentation errors ultimately influence strategic flight plans generated by the planning system. This illustrates the importance of having accurate sensor measurements: a wind model - and hence planned trajectories - can only be as good as the measurements describing the external environment.

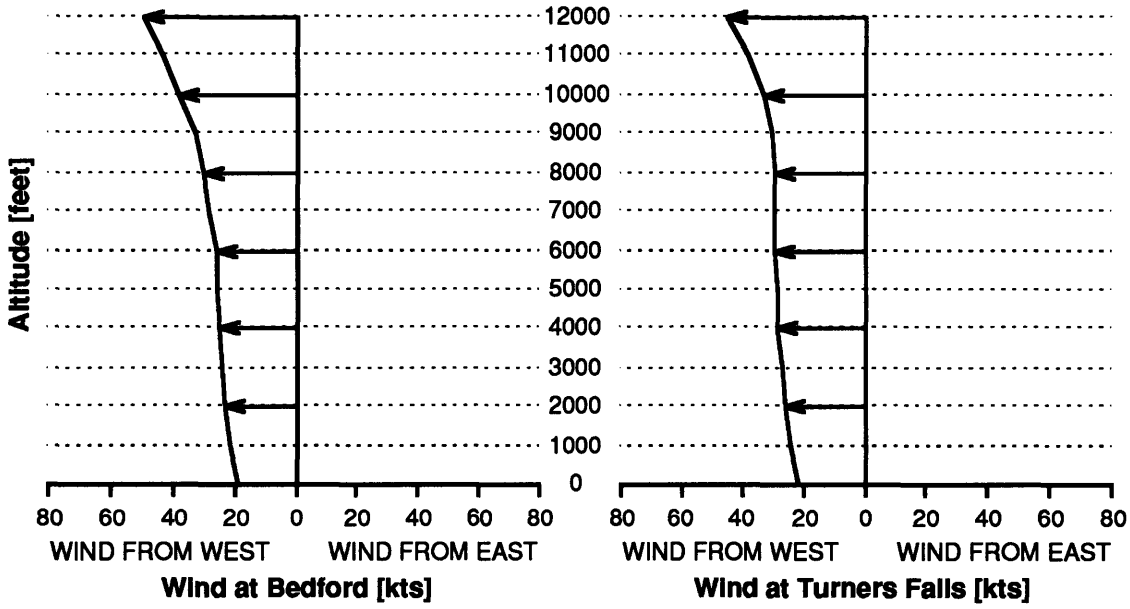

Figure 5.34 Test 1 - Estimated Wind Profile After Three Measurements

Magnetic heading and true airspeed were the most error-prone measurements since the groundspeed vector was sensed by a fairly accurate LORAN receiver. A bias in the airspeed measurement that produces a reading higher than the actual airspeed would explain the observed behavior. (Wind vector estimation errors in the direction of flight are primarily influenced by airspeed, while errors perpendicular to the flight direction are

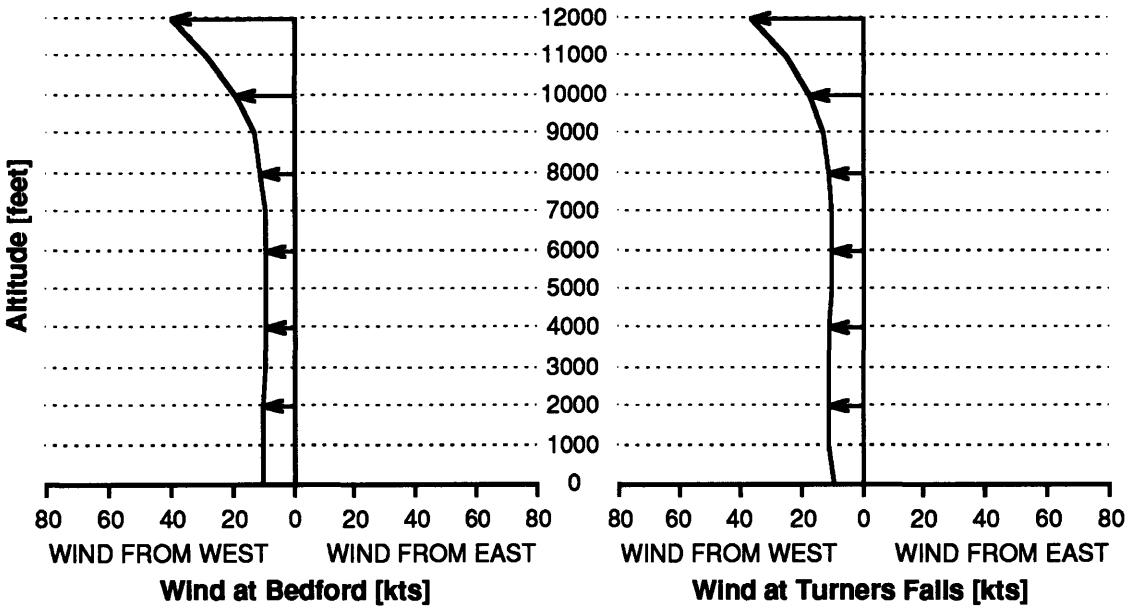

Figure 5.35 Test 2 - Estimated Wind Profile After Four Measurements

caused largely by heading errors.) Since a 25 kt wind was estimated at 6000' at the end of Test 1, while a 10 kt wind was estimated at 6000' at the end of Test 2, a rough estimate of the airspeed error would be 8 knots (half the difference between the two estimates). This represents approximately a six percent error over the 140-knot airspeed range of the test aircraft. Only thorough calibration tests can determine to what extent the measured differences were a result of instrument errors, characteristics of the sensor fusion algorithm, or natural wind variations.

The apparent measurement errors were in spite of extensive calibration tests performed on the air data sensors. This flight test demonstrated that a calibration model developed using data from one flight test may not be valid at a later date; sensor characteristics can drift over time.

5.7.3 Air Data Acquisition

Postflight data analysis identified occasional invalid datapoints in the sensor data stream. Examples of these easily-identified errors included altitudes in excess of 200,000

feet and outside air temperatures greater than 700 degrees Celsius. It could not be determined whether the isolated errors (detected at an average rate of 3.3 errors/hour) were caused by the sensors themselves or by problems with the serial interfaces over which they communicated with the computer. These datapoints were rejected in the postflight analysis. A practical system should employ robust error identification and correction schemes to handle occasional erroneous data. Quality control of incoming data is especially important in a true emergency, where one wrong input to a tactical planning algorithm could cause a dangerously incorrect response.

Sampling and conversion of sensor measurements into a usable form took approximately one third of the total computational time. Implementation of error identification algorithms would require additional computational resources. For this reason, practical planning systems should perform air data sampling, calibration, and correction on a dedicated air data computer.

6 Tactical Planning Tests

This chapter details flight tests performed on December 19th, 1992 that demonstrated the ability of the planning system to function on multiple strategic and tactical levels. The test engineer acted as mission manager for both tests, invoking the tactical planning functions as appropriate.

6.1 Collision Avoidance Planner Test

6.1.1 Procedure

This test was performed to demonstrate the planner's ability to break out of strategic trajectory planning into a tactical mode in response to an unpredicted event - in this case a simulated potential collision with another aircraft. A flight plan to Bedford was generated from a point near Sterling, Massachusetts (approximately 25 nm west of Bedford) at an altitude of 2500'. Figure 6.1 shows wind profiles at Bedford and Sterling estimated by the wind model using National Weather Service forecast data.

Since the winds for this test were generally from the west, the planned flight indicated by the thin dashed line in Figure 6.2 had a cruise altitude of 5500'. (The flight path proceeds from right to left.) At a randomly-chosen point, the flight test engineer simulated a TCAD-generated (or TCAS-generated) traffic hazard indication by manually suspending normal strategic plan evaluation and invoking the collision avoidance planner. The

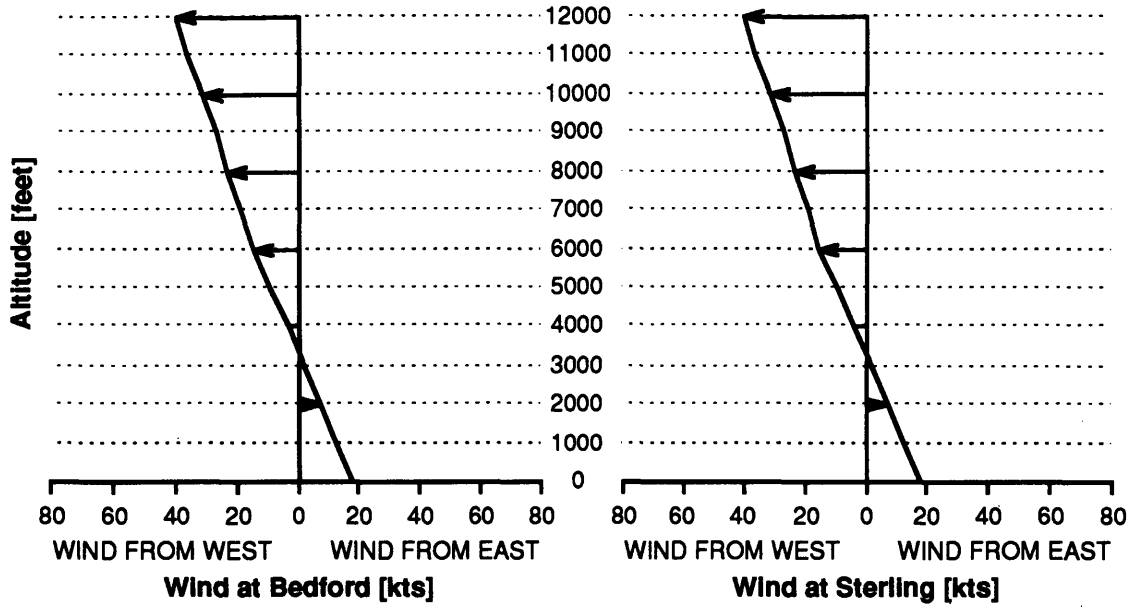

Figure 6.1 Wind Forecast used for Collision Avoidance Planner Test (On this figure, "WIND FROM WEST" and "WIND FROM EAST" are used to indicate wind components along the 87° true course from Sterling to Bedford.)

planner commanded the pilot to "DESCEND AT MAXIMUM PRACTICAL RATE" for collision avoidance. (This command was chosen to emulate a nearby aircraft at an altitude slightly above the test aircraft.) The test aircraft was climbing through approximately 3800' bound for 5500' when the traffic hazard was simulated.

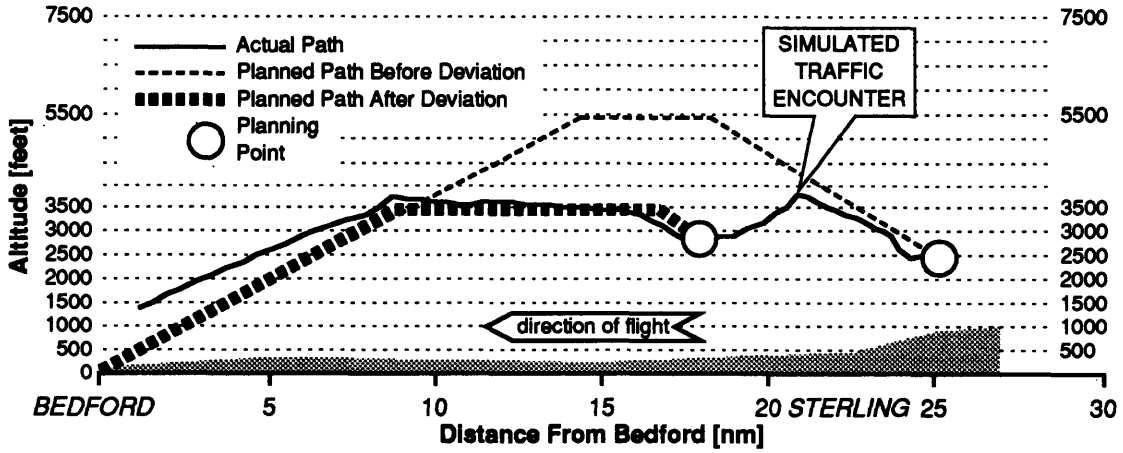

Figure 6.2 Collision Avoidance Planner Test

When the aircraft had descended for approximately 1000', the pilot was told that the collision threat had passed, and the planner was returned to its strategic planning

function. Evaluation of the original flight plan showed that 5500' was no longer the optimum cruise altitude since the aircraft had lost 1000' in deviating from its planned altitude profile; the option to *reacquire* the original flight plan was no longer optimal. Instead, a newly-generated plan was adopted with a cruise altitude of 3500' (shown as a heavy dashed line in Figure 6.2), demonstrating the *replan* option. The new plan was followed until landing at Bedford.

6.1.2 Discussion

This test demonstrated the planning system's ability to respond to a potentially hazardous situation and to return to a strategic planning condition after the tactical deviation. Since the original strategic trajectory was determined to no longer be a viable plan, the trajectory planner was used to generate a new plan. That a new plan had to be generated illustrates a fundamental advantage of performing strategic planning onboard the aircraft; without airborne replanning capability, a system could not react to changes in the external environment.

6.2 Engine-Out Planner Test

A power loss was simulated to demonstrate the system's capacity to provide real-time emergency guidance in the event of an engine failure.

6.2.1 Procedure

This flight test sequence was initiated near the Sterling, Massachusetts airport and proceeded east towards Bedford (from right to left on Figure 6.3). At frequent intervals along the route, the planner was toggled from strategic planning mode into the engine-out planning mode. The engine-out planner evaluated airports at Sterling and Stow, Massachusetts for suitability as landing sites; the zones in which these two airports were found usable for landing are shown.

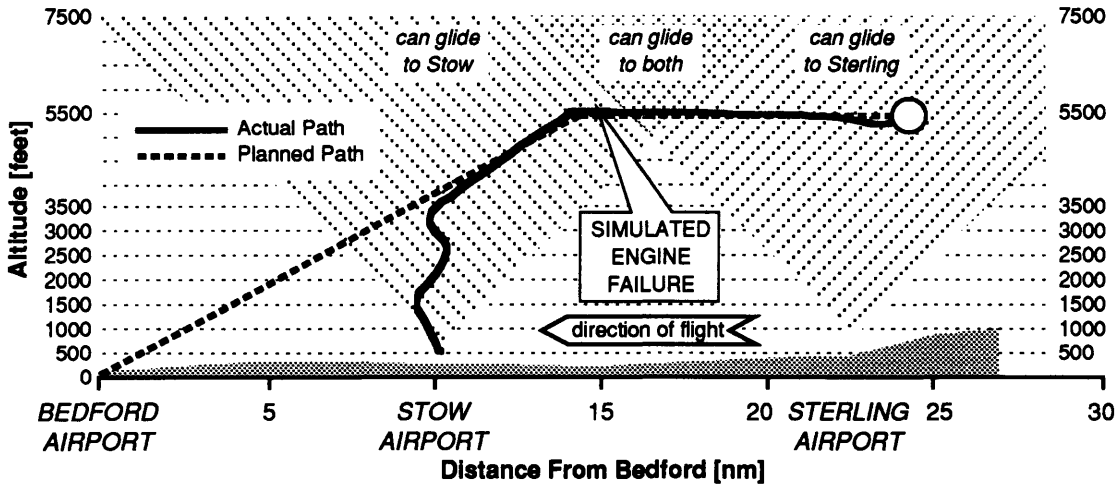

Figure 6.3 Engine-Out Planner Test

Sterling airport was the only modeled landing site available during the first part of the flight. The flight path then passed through a small region in which both airports could be reached in a glide. A simulated engine failure (representing a random, unexpected event) occurred soon after Sterling airport went out of gliding range. After setting the engine power to idle, the pilot was provided with continuous updates of bearing to the Stow airport and the estimated altitude upon reaching the airport (recall that 500' over the airport was required for a landing field to qualify as reachable). The flight profile can be seen to continue at a constant altitude for a small distance after the power was set at idle. During this period, the aircraft was decelerating from its cruise speed of approximately 120 knots to its best-range glide speed of 79 knots. A gliding descent was made until the aircraft was almost directly over the airport with 3000 feet of altitude above ground level. (The overlap of the gliding flight path and the originally planned path was a coincidence.) A circling pattern was then flown to the north of Stow to lose altitude while remaining close to the airport. This pattern can be seen on the map view shown in Figure 6.4, and appears as a "corkscrew" pattern on Figure 6.3. After losing enough altitude to make a final approach, power was reapplied and a runway flyover was performed at Stow.

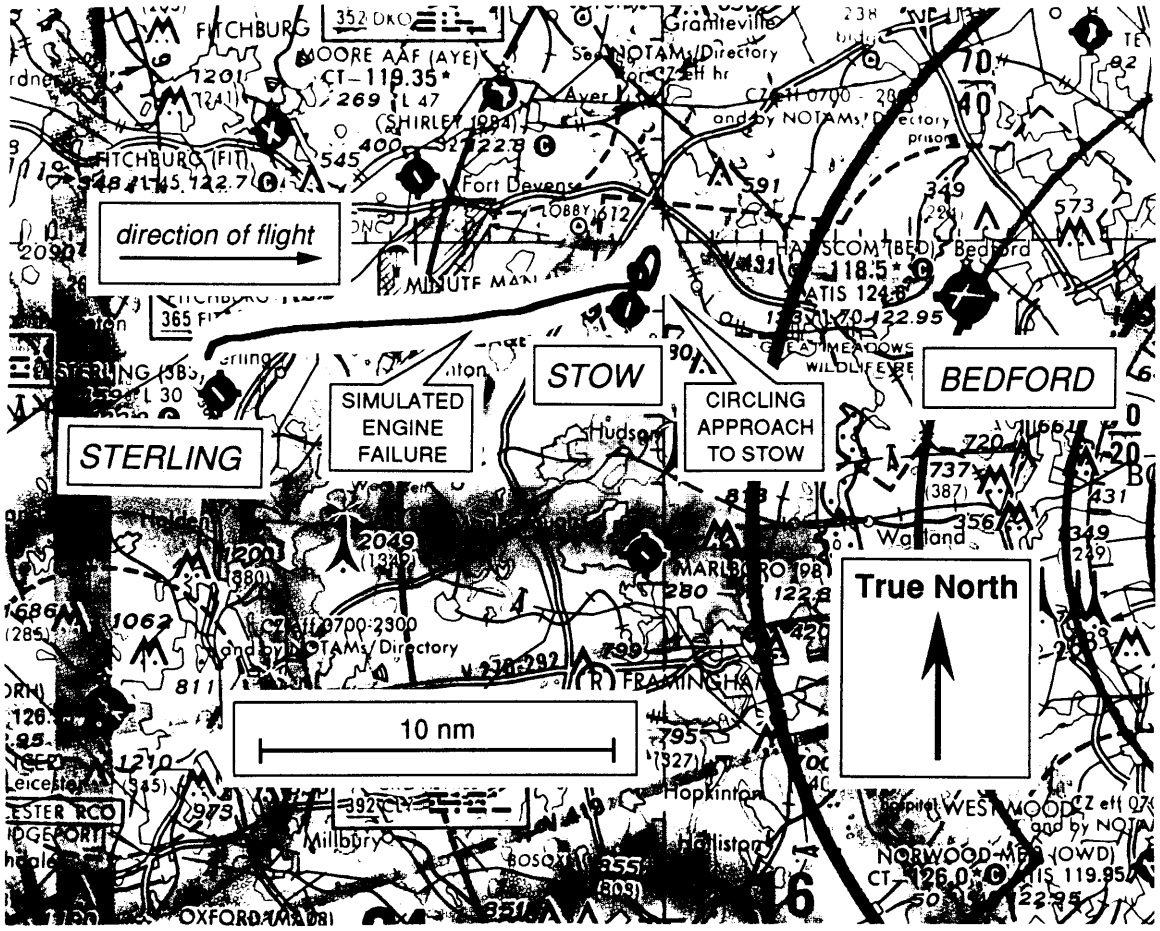

Figure 6.4 Map View of Engine-Out Planner Test
(NOTE: Flight path proceeds from left to right.)

6.2.2 Discussion

The engine-out planner provided guidance to a suitable airport after the simulated engine failure. Tactical planning tests successfully validated the usefulness of the multi-level structure of the planning system developed for this project. More complex tactical and strategic planning algorithms could be implemented without fundamentally changing the nature of this multi-level system. These results hold promise for the implementation of practical systems capable of dealing with flight situations more complex than the ones dealt with in these tests.

7 Conclusion

An automated planning system was implemented on a microcomputer instrumented with air data sensors, and successfully demonstrated in flight tests on a light general aviation aircraft. Multiple levels of strategic and tactical planning were available. Capabilities included minimum-time trajectory generation, and supplying tactical deviations in response to collision hazard and power loss situations. Inputs to the planning process included representation of winds and temperatures aloft, aircraft performance, ground facilities, and terrain.

7.1 Strategic Planning

The strategic planning algorithm used a directed search technique to minimize the cost function of a path through a two-dimensional nodal network. Nodes were distributed in altitude and on the great circle route between the starting and destination points. The plans produced were consistent with the performance of the test aircraft and the estimated wind conditions.

Two improvements were made over existing planning techniques. First, flight legs which included a climb or descent were broken down into separate segments: a level cruise portion and a climb or descent. A *virtual node* was added at the top-of-climb or top-of-descent point, as appropriate, allowing high accuracy in the calculation of flight plan costs. Second, a time penalty was added to the cost function on climb and descent legs to account for unmodeled costs associated with changes in flight condition. This

transition penalty, incorporated as a result of initial flight testing, prevented generation of flight profiles that oscillated between two cruise altitudes.

Additional complexity could be added without changing the fundamental nature of the strategic planning algorithm. Initial simplifications made to make the problem tractable can be removed, allowing flight planning in three dimensions to allow lateral flight deviations. Variable airspeeds and power settings could be modeled and admitted into the flight planning process to achieve more efficient trajectories. Factors such as predicted turbulence and icing regions could also be taken into account. Increased complexity would require additional computational power and efficient planning algorithms such as the A* heuristic search.

7.2 Tactical Planning

Tactical planning was performed to demonstrate the system's ability to handle unexpected hazardous circumstances. After directing a rapid altitude change to avoid a collision with a simulated nearby aircraft, the system's multiple-level structure allowed transition back into a strategic planning mode with reacquisition or replanning options. A successful demonstration was given of the engine-out planner's ability to guide the pilot on a gliding approach to a suitable airport.

In a practical system, sensors will provide real-time information on actual hazards to flight. These will include collision avoidance systems to warn of nearby aircraft, and engine health monitors to provide propulsion system status. Weather radar, lightning detectors (e.g. Stormscope), and icing detectors could all serve as inputs to tactical planning algorithms. Again, the multiple-level structure allows integration of these sensors without fundamentally changing system characteristics.

7.3 Sensor Fusion

Fusion of real-time sensor measurements into a dynamic wind and temperature model was successfully demonstrated. Strategic planning tests initialized with an intentionally-flawed wind forecast showed that the system could quickly adapt flight plans to reflect actual environmental conditions. Wind measurements appeared to depend on the direction of flight, suggesting that an airspeed bias may have corrupted the measurements despite careful calibration. Wind profiles estimated on different aircraft headings were shown to have different characteristics, illustrating the effect of measurement errors on the wind model, and ultimately, on the flight plans generated. These effects highlighted the difficulty of obtaining accurate inflight measurements and the importance of sensor fusion techniques.

Erroneous datapoints were occasionally obtained from the sensor hardware (e.g. altitudes in excess of 200,000 feet). It was determined that error-correction schemes should be employed to identify bad data as a first step in sensor fusion. Quality control of incoming data becomes critically important when the variables being measured are of critical importance to flight safety. For example, errors in measurement of nearby aircraft positions can have disastrous effects on conflict resolution schemes. The increased computational demands of error correction and additional sensors will require a separate computer dedicated to air data acquisition and processing.

7.4 Probabilistic Planning

Probabilistic planning concepts were introduced as a way of dealing with the uncertainty present in models of environmental variables. Accounting for uncertainty can lower expected operational costs by considering many candidate flight plans along with their associated cost probability density functions. A flight plan is adopted based on its probabilistic merit and is flown until evidence builds for adopting a different plan. Such

planning algorithms require probabilistic models of the environmental conditions which influence the cost of a flight (e.g. winds); a probabilistic wind model was developed and is presented in Appendix C. Planning based on a probabilistic world model shows promise for lowering expected operational costs, especially when averaged over many flights. Models and planning algorithms capable of dealing with uncertainty require increases in computing power over the deterministic methods used for this flight test program.

7.5 Summary

This project successfully demonstrated inflight strategic and tactical planning based on a dynamic world model with fused sensor information. Future practical planning systems for pilot decision aiding and primary mission control for autonomous vehicles will employ increasingly complex sensors and computational methods. The multiple-level planning structure demonstrated here is fundamentally capable of dealing with this increased complexity.

References

1. Rose, G.B., "An Application of the Out of Kilter Algorithm Network Flow Algorithm to Least Time Flight Planning." M.I.T. Bachelor of Science Thesis, 1965.

2. Simpson, L., Bashoium, D., and Carr, E., "Computer Flight Planning in the North Atlantic," Journal of Aircraft, Vol. 2, No. 4, July-Aug. 1965.

3. Corrigan, J., and Keller, K., "Pilot's Associate: An Inflight Planning Application," AIAA Guidance, Navigation, and Control Conference, Aug. 1989.

4. Glickstein, I., "Automated Threat Assessment and Response," *American Helicopter Society Annual Forum and Technology Display*, May 1990.

5. Layton, C., Smith, P.J., McCoy, E., and Bihari, T., "Design Concepts for the Development of Cooperative Problem-Solving Systems," Ohio State University internal report, 1990.

6. Adams, M.B., and Hansman, R.J., "Last Hurdle for Autonomous Vehicles," *Aerospace America*, Oct. 1991.

7. Hollister, W.M., Bradford, E.R., and Welch J.D., "Using Radar Tracks to Estimate Winds Aloft," *The Lincoln Laboratory Journal*, Vol. 2, No. 3, 1989.

8. Benjamin, S.G., Brewster, K.A., Brummer, R., Jewett, B.F., Schlatter, T.W., Smith, T.L., and Stamus, P.A., "A 3-Hour Mesoscale Assimilation System Using ACARS Aircraft Data Combined With Other Observations," American Meteorological Society Third International Conference on the Aviation Weather System, Jan. 1989, pp. 117-122.

9. Pearl, J., *Heuristics: Intelligent Search Strategies for Computer Problem Solving*, Addison-Wesley Publishing Company, 1984.

10. Nilsson, N.J., *Principles of Artificial Intelligence*, Tioga Publishing Company, 1980.

11. Niiya, C.K., "An Application of the A* Search Technique to Trajectory Optimization," M.I.T. Master of Science Thesis, 1990.

12. Piper Aircraft Corporation, *Arrow IV Pilot's Operating Handbook*, Nov. 1978.

13. Drake, A.W., and Keeney, R.L., *Decision Analysis Video Course Manual*, Massachusetts Institute of Technology, 1978.

14. Barnes, S.L., "A Technique for Maximizing Details in Numerical Weather Map Analysis," *Journal of Applied Meteorology*, Vol. 3, 1964, pp. 396-409.

15. Sherretz, L., "Developing the Aviation Gridded Forecast System," American Meteorological Society Fourth International Conference on the Aviation Weather System, June 1991, pp. 102-105.

16. Buell, C., "Space Variability of Winds at Aircraft Altitudes," AFCRL-62-273 (II), Proceedings of the National Symposium on Winds for Aerospace Vehicle Design, Vol. 2, Air Force Cambridge Research Laboratories, Mar. 1962.

17. Court, A., "Applying Statistical Representations of Wind," AFCRL-62-273 (I), Proceedings of the National Symposium on Winds for Aerospace Vehicle Design, Vol. 1, Air Force Cambridge Research Laboratories, Mar. 1962.

18. Etkin, B., *Dynamics of Atmospheric Flight*, John Wiley & Sons, 1972.

19. Brown, R.G., Introduction to Random Signal Analysis and Kalman Filtering, John Wiley & Sons, 1983.

20. Nelson, G.G., "Real Time Winds Data for Flight Management," AIAA Aerospace Sciences Meeting, Jan. 1990.

21. Lunnon, R.W., "Short Range Forecasts for Air Traffic Control Using High Resolution Aircraft Data," American Meteorological Society Fourth International Conference on the Aviation Weather System, June 1991, pp. 301-306.

22. den Braven, W., "Design and Evaluation of an Advanced Air-Ground Data-Link System for Air Traffic Control," NASA TM-103899, Jan. 1992.

23. Tobias, L., Volckers, U., and Erzberger, H., "Controller Evaluations of the Descent Advisor Automation Aid," NASA TM-102197, June 1989.

24. Green, S., Davis, T., and Erzberger, H., "A Piloted Simulator Evaluation of a Ground-Based 4D Descent Advisor Algorithm," AIAA-87-2522, AIAA Conference on Guidance, Navigation, and Control, Aug. 1987.

Appendix A - Uniform-Cost Search

The uniform-cost directed search operates by keeping track of the cost $g(n)$ of the cheapest path found to each node n while manipulating nodes between lists called "OPEN" and "CLOSED." When exploring arcs leading away from a given node n, the search considers successor nodes on the level, climb, and descent paths leading away from n. Pointers are used to keep track of the solution path, with successor nodes pointing back to their parent nodes. The uniform cost search algorithm is summarized by the following steps, based on those presented in [Pearl]:

1) Put the start node s on OPEN.

2) If OPEN is empty, exit with failure; no solution exists.

3) Remove the node n from OPEN for which $g(n)$ is a minimum and put it on CLOSED.

4) If n is a goal node, exit successfully. The solution may be later obtained by tracing the path along the pointers from n back to s.

5) Expand node n, generating all its reachable neighbors. If no neighbors are reachable, go to step 2.

6) For each successor node n' of n:

   a) Calculate $g(n')$.

   b) If n' was neither on OPEN or CLOSED, put it on OPEN. Direct the pointer of n' back to n. Assign the newly computed $g(n')$ to node n'.

   c) If n' was already on OPEN or CLOSED, and if the newly computed $g(n')$ is less than the value previously assigned to n', direct the pointer of n' back to n. Assign the newly computed $g(n')$ to node n'. If node n' was on CLOSED, move it to OPEN.

d) If n' was already on OPEN or CLOSED, and if n' already has n as its parent, assign the newly computed $g(n')$ to node n'. If node n' was on CLOSED, move it to OPEN.

7) Go to step 2.

When the cheapest node on OPEN is expanded in step 5, its successor cost $g(n')$ rises above $g(n)$, and other nodes are then selected for further expansion. This causes the costs of the nodes on OPEN to remain roughly the same, giving rise to the name "uniform-cost."

Appendix B - Performance Curves

The following are the performance curves (reproduced from the *Arrow IV Pilot's Operating Handbook* [Piper Aircraft]) for the standard climb, cruise, and descent conditions used by the strategic trajectory planner.

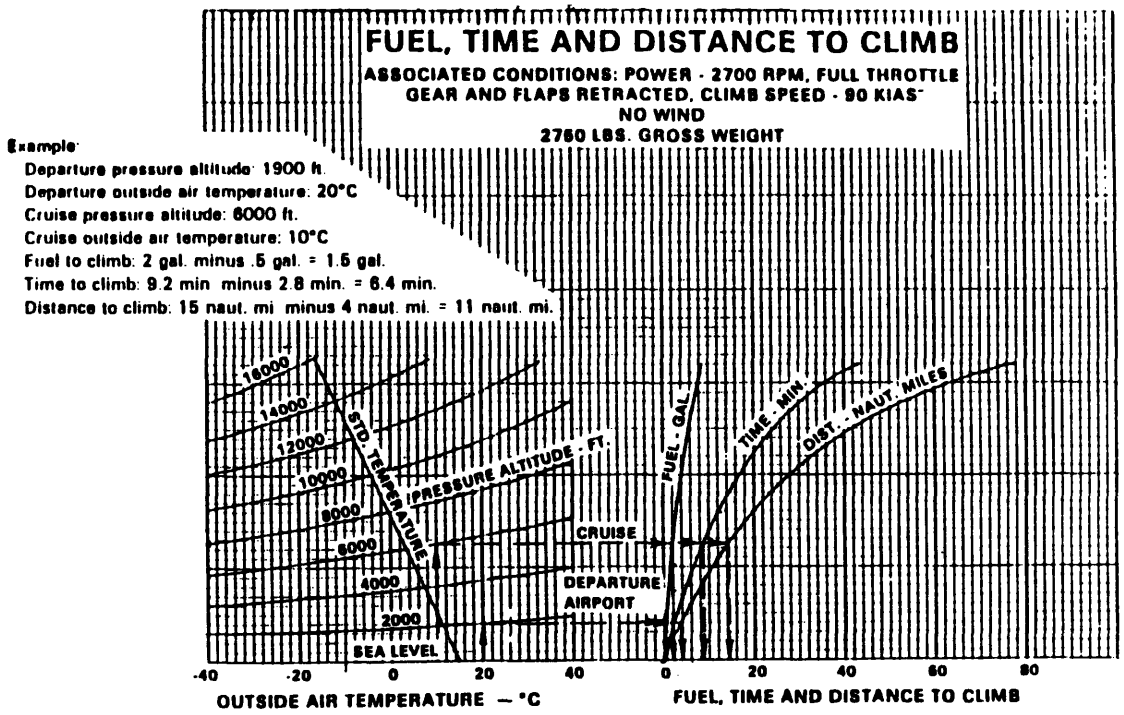

Figure B.1 Fuel, Time, and Distance to Climb

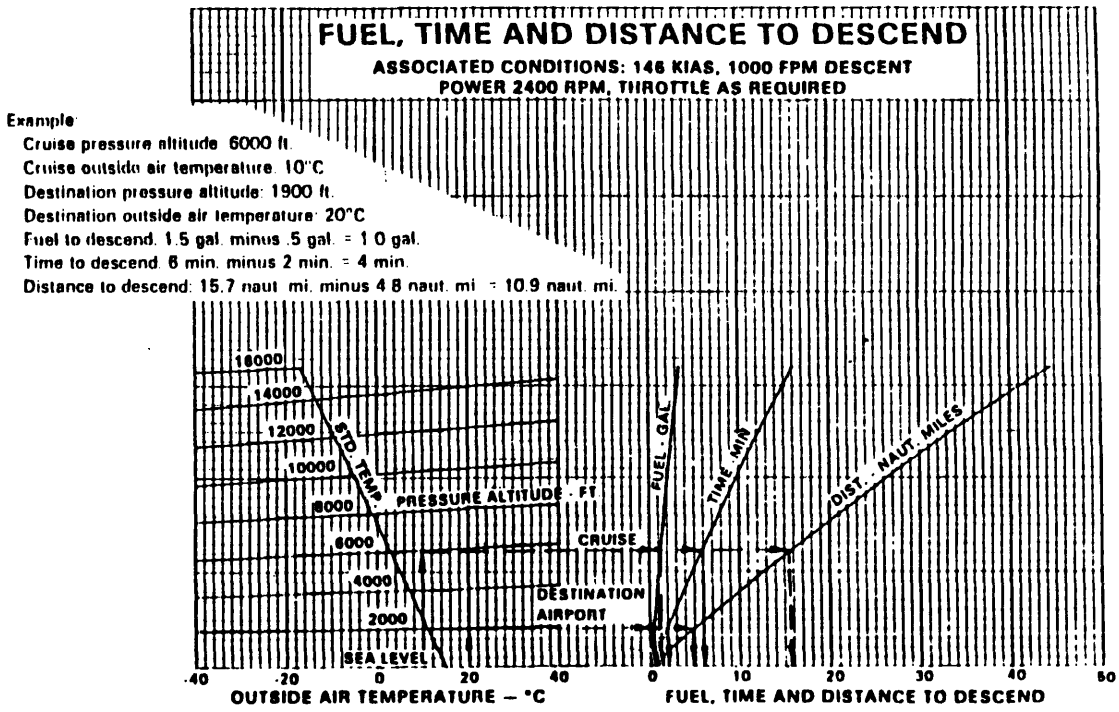

Figure B.2 Speed Power Performance Cruise

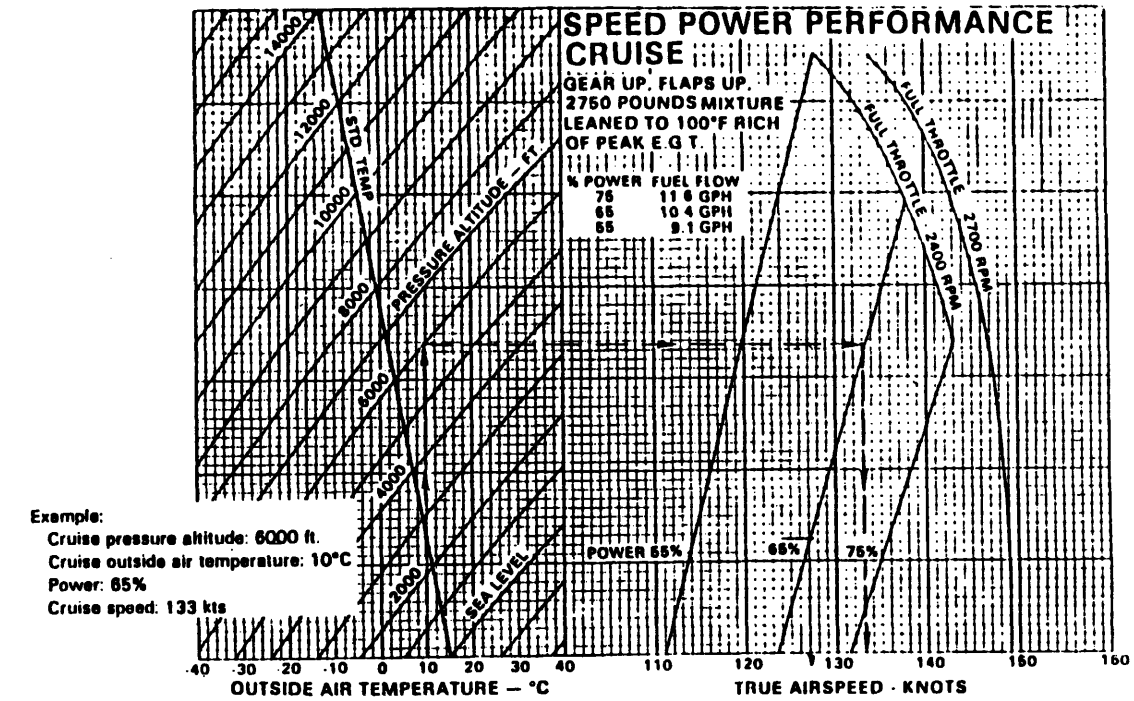

Figure B.3 Fuel, Time, and Distance to Descend

Appendix C - Probabilistic Wind Model

C.1 Introduction

Future flight routing algorithms and Air Traffic Control (ATC) planning systems will benefit from wind representations which take into account uncertainties in the measured and modeled windfield. An algorithm is presented here for fusing multiple datapoints into a single probabilistic "nowcast" or forecast describing the windfield within a prescribed time interval and volume of airspace. This probabilistic windfield representation contains information on the accuracy and interrelationships between the winds at different points and times, and presumes a knowledge of atmospheric properties (process noise and dynamics) and sensor characteristics (sensor noise and dynamics). The advantages of having probabilistic information are demonstrated using two application examples. Sensor sampling rate and digital filtering considerations are also addressed.

C.2 Wind Forecast Representations

Two limitations are made on the scope of the wind forecast model described here. First, only the horizontal components of the windfield are considered because a mean vertical wind component does not significantly affect the flight of an aircraft for flight planning or ATC purposes. (Vertical atmospheric motions, however, do affect the safety and comfort of flight in the form of turbulence, and are also used by numerical weather forecast models.) Second, temperature is not represented, although in practice it affects

aircraft performance and indicated/true airspeed relationships. This is done to simplify the presentation of the basic concepts; temperature can be incorporated by a logical extension of the methods presented here.

The windfield is a vector field continuous both in time and space. The most widely used method for representing the vector windfield in three spatial dimensions and one temporal dimension is the *gridded* model [Sherretz]. In this approach, the user picks a set of times, altitudes, latitudes, and longitudes at which each of the two components of the wind vector is to be described. Choosing the fineness of this forecast "grid" involves several tradeoffs. Closer grid spacing (in time and space) allows a more accurate description of the wind structure, but it places a larger burden on the processing and memory capabilities of the computer storing the forecast. Typical flight planning systems employ grid spacings on the order of a thousand feet in the vertical direction and tens of miles in the horizontal direction. Time intervals between gridpoints tend to be shorter for times near the present, and longer in the future, since the accuracy of weather predictions drops rapidly with time. During events associated with rapidly changing winds, such as frontal passages, it is also desirable to use shorter time spacing between gridpoints.

C.3 The Atmosphere as a Random Process

Current methods of weather forecasting and measurement cannot perfectly predict wind speeds, wind directions, and temperatures. It is therefore important to represent of the *accuracy* of these forecast variables, in addition to their *estimated values*. By modeling the atmospheric variables of interest (here limited to wind speed and direction) as random variables, a probability distribution function (PDF) of these variables may be employed to represent a full forecast description. A simple approach describes each forecast variable and its variance. A more meaningful representation includes information, expressed as covariances between forecast variables, on the interrelationships between datapoints.

Random variations in the windfield can be described in terms of their frequency content with respect to time or some spatial dimension. This is mathematically expressed as a *power spectral density* (PSD) function, a measure of the power associated with wind fluctuations at a given temporal or spatial frequency [Buell]. A PSD function describing atmospheric fluctuations is a tensor function of three spatial frequencies (latitude, longitude, and altitude) and one time frequency. The tensor arises because the PSD definition involves the square of the wind vector, thus yielding a dyadic, or second-order tensor:

$$\theta_{ij}(\Omega, \omega) = \frac{1}{(2\pi)^4} \int_{-\infty}^{\infty} \int \int \int \int E[u_i(\mathbf{r}, t) u_j(\mathbf{r} + \xi, t + \tau)] e^{-i(\Omega \cdot \xi + \omega\tau)} \, d\xi \, d\tau \qquad \text{(C.1)}$$

where θ_{ij} is the (i, j) element in the matrix representation of the PSD tensor, Ω is a vector of the three spatial frequencies, and ω is the time frequency. The i-th and j-th components of the wind fluctuation vector are u_i and u_j, respectively. The integrand is the expected product of u_i at a *reference* point $\mathbf{r}$ and time t, and u_j displaced from the reference by ξ in space and τ in time.

Much research has gone into quantifying the statistics of atmospheric fluctuations [Court, Buell], with the results typically expressed in terms of PSD functions. Shown in Figure C.1, reproduced from [Etkin], is an experimental spectrum of wind speed measured at a fixed location. This PSD function has been integrated over the three spatial frequencies $d\Omega$, leaving a function of temporal frequency only. The vertical axis has been multiplied by frequency so that area under the curve corresponds to power associated with atmospheric fluctuations in a given frequency range.

There are two "lobes" containing significant energy, separated by a gap for periods from about 6 minutes to 3 hours. Energy in the high frequency lobe on the right

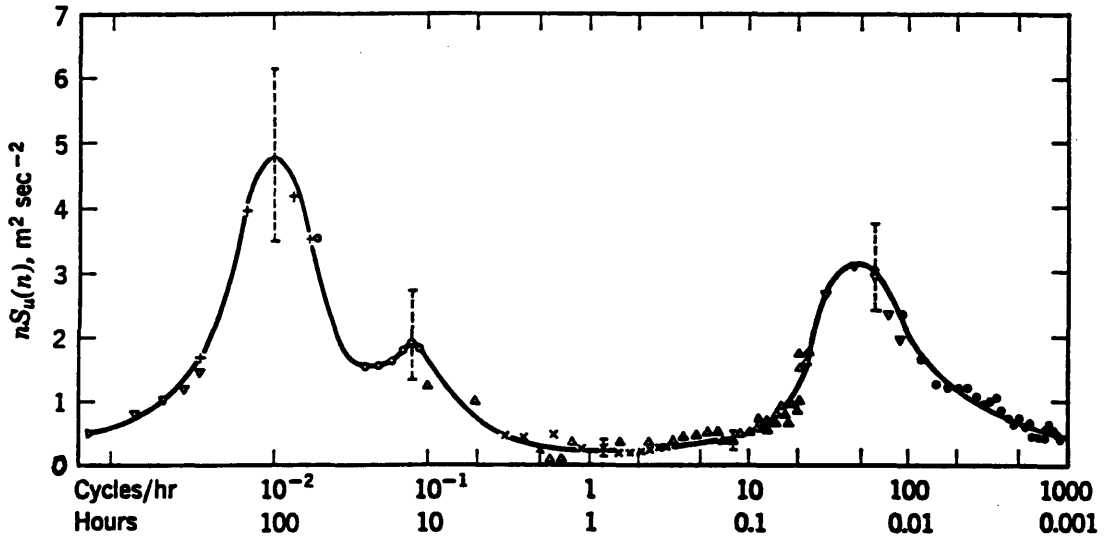

Figure C.1 Experimental Power Spectral Density of Windspeed

is of interest to structural engineers and handling qualities specialists because it represents the turbulence that induces dynamic structural loads on an aircraft. The time scale of these oscillations, however, is not long enough to introduce biases into the flight routing or ATC planning processes; these random fluctuations "balance each other out" over the length of an entire flight segment. The lobe on the left contains energy associated with synoptic atmospheric motions and diurnal wind variations. The gap between lobes suggests that on time scales between a few minutes and a few hours, a high degree of correlation exists at a given location between the winds at different times. This confirms the intuitively known fact that winds usually don't change drastically over short time scales. (There are notable exceptions to this, such as frontal passages, hurricanes, and tornadoes.) The significance of this to flight planning and ATC operations is the following: Current wind measurements provide useful information from the present to a few hours into the future, and are much more reliable than computer-generated winds aloft forecasts that are 12 hours old.

The information expressed by a PSD function in terms of frequency content can also be expressed in terms of spatial and temporal variations using a *correlation function*

[Etkin]. This is defined as the inverse Fourier transform of the PSD and results in a second-order correlation tensor:

$$R_{ij}(\xi, \tau) = E[u_i(\mathbf{r}, t)u_j(\mathbf{r} + \xi, t + \tau)] \qquad \text{(C.2)}$$

R_{ij} is thus the expected product of the i-th component of the wind fluctuation vector at one point and time, and the j-th component at another point displaced in space by ξ and displaced in time by τ. R_{11} and R_{22} are *autocorrelation* functions, while R_{12} and R_{21} are *crosscorrelation* functions. The correlation tensor is generally defined as a function of a reference location **r**, a reference time t, and displacements ξ and τ; however, here R_{ij} is a function only of a vector displacement ξ and a time interval τ. The loss of functional dependence on the reference location and time comes from the assumption that the statistics of fluctuations in the windfield are independent of reference location and time, i.e. that this process is both *homogeneous* and *stationary*.

C.4 The Forecast Vector

A *forecast vector* **x** may be constructed containing all the scalar parameters used in representing a gridded wind forecast. At each grid point (characterized by a latitude, longitude, altitude, and time) the wind vector is defined by a west-east component and a south-north component; these two components are two elements of the forecast vector. Consider an example grid defined over three latitudes, three longitudes, four altitudes, and two times. The forecast vector describing the entire gridded forecast would contain (3 latitudes) x (3 longitudes) x (4 altitudes) x (2 times) x (2 components defining each wind vector) = 144 elements.

The forecast vector elements alone describe the vector windfield over time and space; however, no probabilistic information on the accuracy and interrelationships of these variables is contained in this vector. A complete representation of this information for the example above requires the description of a joint PDF with 144 independent

variables! This method of storing the probabilistic information is clearly computationally infeasible. Fortunately this PDF of the wind process can be approximated as a multivariate Gaussian distribution in most practical applications. The PDF can then be described with the 144-element vector (representing the mean) and a covariance matrix of the same rank.

The elements of the forecast vector covariance matrix Σ are of the form:

$$E[(\textit{one wind perturbation component at a place and time})(\textit{another component at another place and another time})] \quad \text{(C.3)}$$

The equivalence of this interpretation to the definition of a component R_{ij} of the correlation tensor defined above is the key to constructing the covariance matrix relating all the vector elements describing the windfield. To find the covariance of two elements of the windfield vector, the vector difference ξ between locations is evaluated along with the difference τ in times between the two datapoints. R_{ij} is then evaluated with these differences as the arguments ξ and τ to yield one element in the windfield vector covariance matrix. Filling this covariance matrix Σ completes the probabilistic windfield description.

Offline inverse Fourier transformation of experimental PSD functions yields the correlations needed to evaluate elements of the forecast vector covariance matrix. As a rule, these correlation functions decrease as the magnitudes of their arguments ξ and τ increase. This essentially means that the similarity or influence of one wind component, at one place and time, to another component at another place and time, decreases as the distance between them (in space and time) increases.

C.5 Measurement Integration

An intelligent method is desired for integrating new measurements into the existing wind forecast to arrive at a new probabilistic estimate of the present and future

windfield. Sensor error characteristics can be used to establish a model of wind measurement accuracy in the form of a covariance matrix. Thus, a wind measurement is defined by: a [2x1] vector, a [2x2] covariance matrix, and the latitude, longitude, altitude, and time of measurement. The problem within the context of a gridded forecast can be stated: "Given an *a priori* wind forecast vector and covariance matrix AND a wind measurement with its own covariance matrix, generate an *a posteriori* estimate of the present and future windfield." This is essentially a problem of Bayesian estimation in which an a priori vector mean and covariance matrix are updated based on a noisy measurement of a linear combination of elements of the state vector. This procedure appears in the state estimate update step in the discrete-time Kalman filtering algorithm.

Let $\mathbf{x}^-$ be the [nx1] a priori forecast vector mean before a measurement is integrated into the forecast, with [nxn] covariance matrix Σ^-. (n = 144 for the example outlined previously.) Assume an airborne measurement $\mathbf{z}$ (a [2x1] column matrix expressed in east-north coordinates) is taken of the wind vector at a particular place and time. The wind measurement is contaminated by a [2x1] white noise vector θ, with [2x2] covariance matrix Θ (also expressed in east-north coordinates). The structure of Θ is dependent on the sensors used in wind measurement and on the relative geometry of aircraft heading, ground track, and wind direction. The measurement equation is:

$$\mathbf{z} = \mathbf{C}\mathbf{x} + \theta \tag{C.6}$$

The [2xn] matrix $\mathbf{C}$ is called the *measurement matrix* and derives its elements from the linear interpolation algorithm used to retrieve wind data from the forecast. It appears because taking a wind measurement can be interpreted as measuring a linear combination of forecast vector elements. Since most of the vector components in the forecast vector are not at times and places close to where the measurement was made, most of the elements of $\mathbf{C}$ are zero. The only nonzero elements of $\mathbf{C}$ correspond to elements of $\mathbf{x}$ which would be used to interpolate a piece of wind information at the measurement point.

For example, if the gridded forecast is specified every hour on the hour, and the measurement is made at 10:20 PM, there would be nonzero elements in **C** corresponding to the forecast elements at 10:00 PM and 11:00 PM. Since there are four "dimensions" in the forecast grid, a measurement would produce $2^4 = 16$ nonzero elements in **C**.

Bayes' theorem is used to produce updated (a posteriori) estimates of the forecast vector mean, $\mathbf{x}^+$, and its covariance matrix Σ^+. Bayes' theorem is expressed

$$p(\mathbf{x}|\mathbf{z}) = \frac{p(\mathbf{z}|\mathbf{x})p(\mathbf{x})}{p(\mathbf{z})} \tag{C.7}$$

where $p(\mathbf{x})$ is the a priori PDF of the wind forecast vector $\mathbf{x}$ and $p(\mathbf{x}|\mathbf{z})$ is the a posteriori PDF of $\mathbf{x}$, with vector mean $\mathbf{x}^+$ and covariance matrix Σ^+. The following method for calculating this PDF is equivalent to the update step in a discrete-time Kalman filter as outlined in [Brown]. First a [nx2] Kalman gain matrix is computed from

$$\mathbf{K} = \Sigma^-\mathbf{C}^T(\mathbf{C}\Sigma^-\mathbf{C}^T + \Theta)^{-1} \tag{C.8}$$

Note that although **C** is [2xn] and Σ^- is [nxn], the quantity $(\mathbf{C}\Sigma^-\mathbf{C}^T + \Theta)$ is a [2x2] matrix, keeping the matrix inversion in this step computationally inexpensive. The forecast vector and covariance matrix are updated using:

$$\mathbf{x}^+ = \mathbf{x}^- + \mathbf{K}(\mathbf{z} - \mathbf{C}\mathbf{x}^-) \tag{C.9}$$

$$\Sigma^+ = (\mathbf{I} - \mathbf{K}\mathbf{C})\Sigma^- \tag{C.10}$$

The covariances in Σ^+ should in general be smaller than those in Σ^-, since new information improves the forecast estimate.

This algorithm also permits fusion of multiple wind measurements into the forecast in one computational step. These measurements could come from one aircraft making periodic measurements along its flight path, or from multiple aircraft widely

separated from each other. Several researchers have proposed sharing of measurements (via datalink) made by streams of climbing and descending aircraft, so that the winds at each grid altitude are sampled every few minutes [Nelson, Lunnon, den Braven]. Winds aloft can be measured with wind profilers, sounding balloons, and even estimated on the ground from aircraft radar tracks [Hollister et al.]. Rather than incorporate each measurement as it is received, the multi-sensor fusion algorithm in practice would be run as a simultaneous batch process. At each algorithm step, all measurements (with respective error covariance matrices) made since the last batch integration would be fused into the wind forecast to generate a new forecast. To do this with more than one measurement, the components of the measurement equation $\mathbf{z}$, $\mathbf{C}$, and Θ are augmented to include all measured wind vector components. For instance, if there are m measurements, $\mathbf{z}$ becomes a [$2m$x1] column vector. The measurement matrix $\mathbf{C}$ is also augmented to [$2m$xn] to reflect multiple measurements. Finally, Θ will contain independent [2x2] blocks describing the (independent) errors of the different measurements on its diagonal, and zeros outside of these blocks.

C.6 Application Examples

C.6.1 Top of Climb Point Prediction

A typical problem in flight planning, either from the aircraft's or ATC's point of view, is that of estimating the top-of-climb (T/C) point for an aircraft climbing from one altitude to another. Given the horizontal route of flight, the initial altitude and position, and the destination altitude, the goal is to determine the aircraft's horizontal position upon reaching its intended altitude. This position depends largely on the climb speeds used and the winds encountered during the climb. This example will assume that known schedules of climb rate and true climb airspeed (more exactly, its horizontal component) as a function of altitude are followed by the climbing aircraft. (The dependence of these

schedules on temperature will be neglected for now and discussed later.) Consider the following example:

> An aircraft has departed its airport of origin and is climbing out of the terminal area from 2000 feet to 10000 feet. Its climb rate varies linearly from 4000 feet per minute (fpm) at 2000 feet altitude to 2400 fpm at 10000 feet. The horizontal component of true airspeed varies from 255 knots at 2000 feet to 295 knots at 10000 feet. (These numbers are typical for an airliner constrained to fly at an *indicated* airspeed of 250 kts below 10000 feet.)

The problem will be separated into four altitude segments; more segments could be used for greater accuracy. Each segment has associated with it an average rate of climb and an average TAS, as summarized in Table C.1.

Table C.1 Example Altitude Segment Breakdown

SEGMENT ALTITUDE [ft]	CLIMB RATE [fpm]	AVERAGE ROC [fpm]	TAS [kts]	AVERAGE TAS [kts]
2000-4000	4000-3600	3800	255-265	260
4000-6000	3600-3200	3400	265-275	270
6000-8000	3200-2800	3000	275-285	280
8000-10000	2800-2400	2600	285-295	290

The probabilistic wind forecast is used to find the along-track component of the wind in each altitude segment. An average tailwind $\overline{TW_i}$ over each segment is found by extracting from the forecast the *along-track* wind component at the midpoint altitude for each segment. For instance, the tailwind over the second altitude segment would equal the wind vector at 5000 feet dotted with a unit vector pointed in the direction of the desired ground track. It is necessary that the wind vectors for all altitude segments be extracted from the wind forecast at the same time; this the only way to preserve covariance information between winds at different altitudes. The mean vector of segment tailwinds $\overline{\mathbf{TW}}$ and its covariance matrix $\Sigma(\mathbf{TW})$ are extracted by multiplying the forecast vector $\mathbf{x}$ and its covariance matrix Σ by a suitable extraction matrix $\mathbf{E}$

$$\overline{\mathbf{TW}} = \mathbf{Ex} \tag{C.11}$$

$$\Sigma(\mathbf{TW}) = \mathbf{E}\Sigma\mathbf{E}^{\mathsf{T}} \tag{C.12}$$

Expressions for along track groundspeed and time spent climbing in the i-th altitude segment can be written

$$GS_i = TW_i + TAS_i \tag{C.13}$$

$$t_i = \frac{ST_i}{ROC_i} \tag{C.14}$$

Where ST_i is the i-th segment thickness. (For Equation C.13 to be strictly true, the wind vector must be aligned with the ground track, so that this expression is suitable for small wind crab angles. Generalizing the problem to include wind vectors with a significant cross-track component will be discussed later.) The horizontal distance covered on a segment is

$$d_i = t_i(GS_i) = t_i TW_i + t_i TAS_i \tag{C.15}$$

And the distance covered during the entire climb is:

$$d_{T/C} = \sum_{i=1}^{4} t_i TW_i + t_i TAS_i = \mathbf{t}^{\mathsf{T}}\mathbf{TW} + \mathbf{t}^{\mathsf{T}}\mathbf{TAS} \tag{C.16}$$

Where **t**, **TW**, and **TAS** are vectors containing segment times, tailwind components, and true airspeeds. The only random element on the right hand side of the above equation is **TW**. The mean and variance of random variable $d_{T/C}$ may finally be calculated using the rules for linear combinations of multiple random variables:

$$\overline{d_{T/C}} = \mathbf{t}^{\mathsf{T}}\,\overline{\mathbf{TW}} + \mathbf{t}^{\mathsf{T}}\mathbf{TAS} \tag{C.17}$$

$$\sigma^2(d_{T/C}) = \mathbf{t}^{\mathsf{T}}\Sigma(\mathbf{TW})\,\mathbf{t} \tag{C.18}$$

It is evident that the off-diagonal terms of $\Sigma(\mathbf{TW})$ that represent covariances between tailwinds at different altitudes do indeed affect the T/C point prediction. Thus it is important to generate them at the time wind components are extracted from the wind forecast. Positively correlated wind components will result in a larger variance in T/C distance than predicted by a model with no correlation information. Certain combinations of positively and negatively correlated tailwind components at different altitudes could combine to produce smaller variances than predicted by a no-covariance model.

This same technique, here applied to a climb situation, can be used to determine a desired top-of-descent (T/D) point for an aircraft descending into a terminal area. This problem is of great interest to ATC researchers [Tobias et al., Green et al.]. The example here illustrates an advantage of knowing the variance of the estimated T/C or T/D point: the routing algorithm can generate trajectories that will put the aircraft at the final altitude before the T/C or T/D point with a specified degree of confidence. For example, predicting a T/D point too close to the destination airport can prove costly; if the aircraft experiences stronger tailwinds (or weaker headwinds) than the wind forecast predicted, the aircraft will have too much altitude at the end of the descent and may have to be rerouted. If the mean predicted T/D point as predicted by the method above is used, this situation will theoretically occur half the time. Instead, a T/D point *before* this mean can be used to ensure that the aircraft is at the desired altitude at the desired geographical location with, for instance, an 80% level of confidence. This point in the distribution can be found by integrating under the Gaussian describing $d_{T/D}$ to find the T/D point which gives a 20% chance of having too much altitude at the destination.

C.6.2 ETA Prediction

The second application of the probabilistic wind representation is used to predict ETAs (and their covariances) along a string of waypoints. Consider a flight consisting of s segments. The segment distances can be put into a [sx1] vector **d** where the time spent on a particular segment is

$$t_i = \frac{d_i}{TAS_i + TW_i} \tag{C.19}$$

Note that the segments do not all need to have the same ground track. When the [sx1] vector **TW** is extracted from the wind forecast, a different ground track unit vector is simply dotted with each predicted wind vector to arrive at a segment tailwind component.

The expression in equation (C.19) is nonlinear in TW_i. This is problematic since this analysis depends on being able to express the desired quantities (waypoint ETAs) as linear functions of the random variables affecting the problem (tailwind speeds). The solution is to linearize the expression for time spent on a segment around a mean tailwind. Writing the tailwind as its constant mean and a perturbation:

$$TW_i = \overline{TW_i} + \delta TW_i \tag{C.20}$$

leads to the following expression for time spent on the i-th segment linearized using a first-order Taylor series about the mean:

$$\begin{aligned} t_i &= \frac{d_i}{TAS_i + \overline{TW_i}} - \frac{d_i}{(TAS_i + \overline{TW_i})^2}\delta TW_i \\ &= \frac{d_i}{TAS_i + \overline{TW_i}} - \frac{d_i}{(TAS_i + \overline{TW_i})^2}(TW_i - \overline{TW_i}) \end{aligned} \tag{C.21}$$

which simplifies to

$$t_i = \frac{-d_i}{(TAS_i + \overline{TW_i})^2} TW_i + \frac{d_i TAS_i + 2d_i\overline{TW_i}}{(TAS_i + \overline{TW_i})^2} \tag{C.22}$$

Note that the first term on the right hand side of equation (C.22) is linear in TW_i, while the second is constant. The notation can be simplified by a constant square diagonal [sxs] matrix **A** and a constant [sx1] vector **b** defined by

$$A_{ii} = \frac{-d_i}{(TAS_i + \overline{TW_i})^2} \quad ; \quad A_{ij} = 0 \quad \text{for } i \neq j \tag{C.23}$$

$$b_i = \frac{d_i TAS_i + 2d_i \overline{TW_i}}{(TAS_i + \overline{TW_i})^2} \tag{C.24}$$

The [sx1] vector **t** of times spent on each segment can now be written

$$\mathbf{t = A\ TW + b} \tag{C.25}$$

The ETA at the end of a given segment is the sum of the times spent on that and all previous segments. Thus the [sx1] vector **ETA** of arrival times at the end of each segment can be written

$$\mathbf{ETA} = \begin{bmatrix} 1 & 0 & 0 & 0 \\ 1 & 1 & 0 & 0 \\ 1 & 1 & 1 & 0 \\ 1 & 1 & 1 & 1 \end{bmatrix} \begin{bmatrix} t_1 \\ t_2 \\ t_3 \\ t_4 \end{bmatrix} = \mathbf{L\ t = L\ A\ TW + L\ b} \tag{C.26}$$

Finally, the vector mean and covariance matrix of estimated arrival times at segment endpoints are

$$\overline{\mathbf{ETA}} = \mathbf{L\ A\ \overline{TW} + L\ b} \tag{C.27}$$

$$\Sigma(\mathbf{ETA}) = \mathbf{L\ A\ \Sigma(TW)\ A^T L^T} \tag{C.28}$$

C.7 Limitations

Several important factors were ignored in the preceding application examples. One is the effect of temperature variations on the aircraft's flight speeds and climb rates. For example, an aircraft's climb rate versus altitude schedule depends on the temperatures encountered during the climb. A full atmospheric model would include a

representation of temperature in addition to the wind vector, along with covariances relating the two. Temperature would then be incorporated into the equations governing the quantities of interest (T/C point, ETAs, etc.) as a random variable. An extension of the technique presented would involve linearizing about the mean of the meteorological forecast vector (now including temperature information), resulting in an expression for $d_{T/C}$ expressed as a linear combination of forecast variables.

Another effect neglected is that of large crab angles (the angle by which an aircraft's heading differs from its desired ground track to compensate for wind). This is usually not significant unless the magnitude of the cross-track wind component is relatively large compared to the true airspeed. Thus, it can become important for slower airplanes flying in high winds, or even for jet aircraft flying perpendicular to the prevailing wind direction at high altitude. As long as the quantities of interest can be represented by a valid linear combination of forecast variables, these quantities and their covariances can be estimated.

C.8 Sampling Rate Considerations

Since atmospheric fluctuations above a certain frequency range have a diminished effect on flight planning, wind measurements should be filtered to prevent degradation by turbulence associated with the high-frequency lobe of the windspeed PSD function shown in Figure C.1. A typical digital lowpass filtering algorithm would produce a weighted average of samples taken over a suitably long period. The time between samples may be small, provided the averaging window is long enough to include at least one full period at the filter cutoff frequency. Also, the air data sampling rate should be fast enough to provide several samples during this averaging period. The filter cutoff frequency should be set low enough to reject oscillations due to aerodynamic modes and structural vibrations. Since the phugoid mode typically has the longest period (ranging from 20 to

90 seconds for most subsonic aircraft) the averaging window should last at least one phugoid period.

C.9 Conclusion

Deterministic representations of the atmosphere generated from numerical forecast models will not meet the needs of the future air transportation system. Instead, multi-sensor, multi-location measurements will be fused into accurate nowcasts and forecasts of meteorological parameters. Information on the variability of these values, and their interrelationships, will be needed to quantify and predict the uncertainty associated with the flight planning process. The forecast model provides an outline for multi-sensor fusion of wind measurements into a probabilistic representation of the windfield over a desired region of space and time, and the examples provide a basis for application to flight planning and ATC problems.